International Journal of Science Academic Research
Vol. 06, Issue 06, pp.10202-10225, June, 2025
Available online at http://www.scienceijsar.com

ISSN: 2582-6425

Research Article

EFFECT OF HEAT TREATMENT TEMPERATURE AND QUENCHING COOLING RATE ON MECHANICAL PROPERTIES OF WROUGHT AL-MG-SI ALLOY (6082AL)

***REN XU, XuBiao and Xiang Yun**

Ping Xiang University 211 Ping An North Avenue, Pingxiang City, Jiangxi Province, China

Received 18th April 2025; **Accepted** 24th May 2025; **Published online** 20th June 2025

Abstract

Due to a series of excellent properties, aluminum alloy materials are widely used in aerospace, transportation, building decoration, packaging containers, machinery and electrical appliances, electronic communications, petrochemicals, energy power, sports and health and other industries, and become an important basic material for the development of the national economy. . Therefore, in recent decades, deformed aluminum alloys have generally developed in two directions. One is to develop new high-strength and high-toughness aluminum alloy materials to meet the needs of aviation and aerospace; the other is to develop a series of civilian aluminum that can meet various conditions of utilization of alloy. Therefore, the improvement and development of aluminum alloy materials is always accompanied by heat treatment and composition development. Heat treatment is one of the most important means to improve the process performance and service performance of the alloy and give full play to the potential of the material. The most commonly used heat treatments for wrought aluminum alloys are annealing, solution treatment, and aging. Deformation heat treatment is also used, and chemical heat treatment is less used. In the production process of aluminum alloy materials, it is necessary to master the basic principles and influencing factors of various heat treatments in order to correctly specify the production process, solve the relevant problems in production, and achieve high quality and high yield. In the end, 6082 aluminium alloy's quenching sensitivity of for rail transport was studied by using end quenching (JEQ) experiment, using JMatpro7.0 simulation software, combined with hardness, tensile property testing and transmission electron microscopy (TEM) observations. The results show that: (1) The TTT curve simulated by JMatpro7.0 shows that the quenching sensitive temperature range of 6082 aluminum alloy is 220~425°C, and the nose peak temperature of β and β'' phases is 375°C. The CCT curve of the alloy shows that so as toinhibit the precipitation of β' (metastable phase) during the quenching process, the quenching cooling rate of the alloy must be greater than 6 °C/s; (2) With the increase of the end quenching distance D, the aging of 6082 aluminum alloy The as-state hardness and strength decreased, and the hardening depth was 23 mm; (3) With the decrease of the quenching cooling rate, the quenching-induced precipitation phase β was preferentially precipitated on the α-(AlMnFeSi) phase at the heterogeneous nucleation site, and in the succeeding aging process doesthe β phase grow and absorb the surrounding solute atoms so that the β'' of theprecipitation-strengthening phase in the grain decreases; (4) In the sluggish cooling process, the vacancy concentration near the grain boundary reduces, and the precipitation-free precipitation zone (PFZ) at the grain boundary expands.

Keywords: Heat treatment, composition, mechanical properties, microstructure, 6082 aluminum alloy, end quenching.

1. Introduction

The improvement of the level of social development has put forward higher requirements for the innovation and development of production technology. It is very important to develop new industrial production technology to apply it scientifically. Aluminum alloy is a relatively important application material in social development. The use of advanced technology in the process of aluminum alloy processing can effectively improve the quality of the material. The processed aluminum alloy can be used in many aspects. In particular, the deformed aluminum alloy 6082 has the advantages of high cost performance, low process requirements but good performance. It is widely used in the construction industry, automobile industry, machinery and so on. Special heat treatment technology to adjust and improve its mechanical properties has special uses for the machinery industry.

2. Relationship between chemical composition and heat treatment temperature of wrought aluminum alloy 6082

2.1 Chemical composition of wrought aluminum alloy 6082

Chemical composition:

Si：0.7-1.3，Fe:≤0.5,Cu:≤0.1,Mn:0.4-1.0,Mg:0.6-1.2,Cr:≤0.25,
Zn:≤0.2,Ti:≤0.1[1].

6082 belongs to the aluminum-magnesium-silicon system. Among these alloys, 51S (magnesium 0.6%, silicon 0.9%) appeared first. Mg_2Si plays a decisive role in the strengthening of aluminum-magnesium-silicon alloys. Looking at the alloys on the Al-Mg_2Si pseudo-binary state diagram (Fig. 1-1) and the alloys containing excess magnesium or silicon, it is found that the aging

Corresponding Author:** ***REN XU,
Ping Xiang University 211 Ping An North Avenue, Pingxiang City, Jiangxi Province, China.

strengthening of the alloy increases with the increase of the number of Mg_2Si phases incorporated into the solid solution during quenching and heating. Mg_2Si It is the main strengthening phase of this alloy. Later studies found that the 51S alloy was not aged immediately after quenching, and stayed for a period of time, which would reduce the subsequent artificial aging effect. In order to compensate for this loss, a small amount of copper and manganese are added on the basis of 51S alloy. Manganese is added to the alloy to refine the recrystallized grains and expand the upper limit of the quenching temperature, thereby increasing the strength of the alloy. The addition of copper significantly improves the plasticity of the alloy during hot working and increases the heat treatment strengthening effect. The addition of copper can also suppress the extrusion effect and reduce the anisotropy of the alloy due to the addition of manganese.

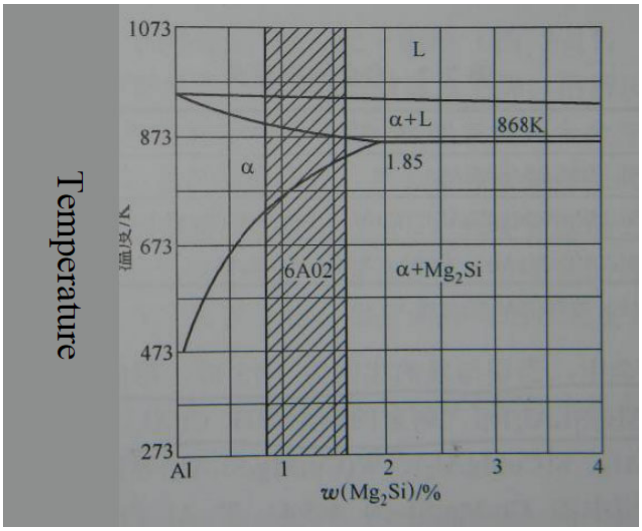

Figure 1-1 Al-Mg_2Si pseudo-binary equilibrium diagram

To increase the strength, increase the silicon content by 1.1-1.25%. But excess silicon can also affect performance because free silicon is produced.

The cast crystals of the alloy ingots are not eliminated, and the tendency of the products to form coarse crystals is prevented. 0.02%-0.1% titanium and 0.01%-0.2% chromium are added to the alloy.

In summary, the improved ingredients are:

Si : 1.15-1.25, Fe:0.2-0.3,Cu:0.05-0.08,Mn:0.4-1.0,Mg:0.9-1.0, Cr:0.1-0.2,Zn:≤0.05,Ti:0.05-0.08.

2.2 Heat treatment temperature

These alloys have a common strengthening phase, Mg_2Si. After quenching, it can be naturally aged or artificially aged. Due to the slow precipitation of the strengthening item Mg_2S at room temperature, the effect of natural aging is not large, and it must be artificially aged to have a high strengthening effect. According to historical records: when silicon and magnesium in the alloy are artificially aged, the silicon phase (Mg_2S, W phase) is preferentially formed. At room temperature, silicon remains in a (Al) supersaturated solid solution and is not easy to precipitate.From Table 1-1, it can be seen that when quenched to 180oC, artificial aging for 5min, and then artificial aging after 48H interval, can obtain greater mechanical properties. And under the normal composition, the solution temperature is 525±5℃, and the holding time is 1-4H. The aging temperature is 165±5℃, and the holding time is 6-8H.

However, for the improved components, due to the increase of Si content, the solution temperature and aging temperature will also change: the solution temperature is 545±5°C, and the holding time is 1-3H. The aging temperature is 175±5°C, and the holding time is 8-12H. It should also be noted that the aging should be done immediately after solid solution, otherwise the mechanical properties will drop a lot. If the residence time exceeds 4 hours, it should be artificially aged for 24 hours. Otherwise there will be a "parking effect". The effect of parking on the degree of reinforcement is shown in Figures 1-2.

Table 1-1 Effect of placement time before artificial aging on mechanical properties

Time interval between quenching and artificial aging	Mechanical Character			Remark
	Tensile strength R*m*(MPa)	Yield strength R*p*2(MPa)	Elongation A%	
Immediately after quenching, artificial aging at 180°C for 5 min and then at an interval of 48H	343	285	13	Artificial aging system 165±5℃ Keep warm for 8h
Quenching 175°C/8h artificial aging	325	273	17	

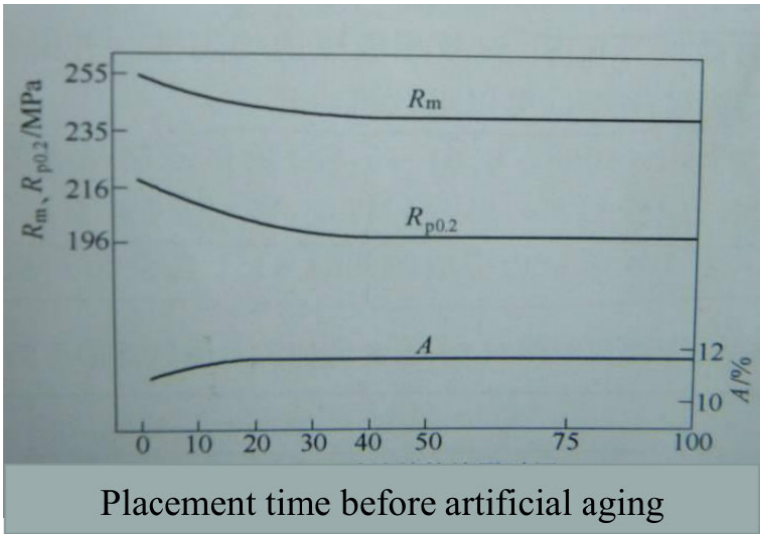

Figure 1-2. The effect of parking time on the performance of 6082 products

2.3 Summary of the relationship between chemical composition and heat treatment temperature

When the chemical composition of 6082 is low, the heat treatment temperature is low, and the solution temperature is 525±5℃. However, when the chemical composition is high, the heat treatment temperature is high, and the solution temperature is 545±5℃.

3. The relationship between heat treatment temperature and low magnification structure and high magnification structure of forged aluminum alloy 6082

3.1 Microstructure and properties of quenched and aged states

Heat treatment can strengthen deformed aluminum alloy products. The structural properties of its quenched and aged state are the basis for its use. Three following aspectsshould be understood: 1. The composition of residual secondary crystals and the content, size and distribution of a small amount of impurities in the alloy; 2. The static recrystallization and the original dynamic recrystallization of the alloy formed by high temperature heating after solution treatment Changes in grains and substructures; 3. The structural characteristics of alloys formed by natural aging or artificial aging.

Heating of deformed aluminum alloy products before quenching makes the soluble strengthening phase, that is, residual secondary crystals (such as $CuAl_2$, S ($CuMgAl_2$, Mg_2Si), etc., dissolved in a (Al) to the maximum extent. Therefore, the structure of the product in the newly quenched state. It is because the compound is significantly reduced than that before quenching and heating, and the impurity phases such as Fe and Si (such as $FeAl_3$, α(AlSiFe), AlMnFeSi, etc.) are refined accordingly. If the alloy contains elements such as manganese, chromium, etc., the α(Al) matrix There are also compounds formed by them and aluminum ($MnAl_6$, $CrAl_7$), etc. All the above-mentioned compounds are indistinguishable from each other. The distribution state on the α(Al) matrix varies with the processing method and deformation process of the product, and can be combined with each other. Analysis of the impact of processing methods on the organization.

Since the heating during the solution treatment before quenching causes the α(Al) solid solution to recrystallize, there are two types of recrystallization at this time: one is that the dynamic recrystallization structure that has been formed during hot working is more fully carried out, or the grains grow; the other is the recrystallization of the α(Al) solid solution that has been dynamically recovered (the recrystallization at this time can be considered as static recrystallization). Normal quenching and aging state α(Al) solid solution recovery subgrain and crystals have fine grain boundaries. In actual production, due to the uniformity and distribution of solid solution components in the alloy, as well as the fluctuation of process parameters during the deformation process, the physical deformation of the alloy during processing and deformation is uneven, and the distribution of distortion energy is also very uniform. The growth and merger of the grains are always realized by the large grains swallowing the small grains, and the grain boundaries move in the direction of the center of curvature. When the grains grow, the progress of the grain boundaries is uneven due to uneven stress distribution. , and are not synchronized, so most of them form "tooth-shaped" grain boundaries. This phenomenon of alloy products is more obvious than that of industrial pure aluminum, especially alloys containing manganese, chromium and pickaxe. For alloys containing copper and zinc, there are also different color contrasts between crystal grains. The greater the contrast, the more sufficient the solid solution of the alloy is. After the solid solution heating of the processed product is completed, in order to prevent the grain boundary from being dissolved, it must be quickly immersed into the cold water, and the transfer time should not exceed 25-30 seconds. Under normal circumstances, the quenching water temperature should not exceed 30^{o}C. In order to prevent distortion or even cracks of large parts and products with complex shapes, the water temperature can be appropriately adjusted to 30-50^{o}C.

3.2 The relationship between heat treatment temperature and time and low magnification

When the solution temperature of 6082 aluminum alloy is 525±5°C, the low magnification structure has no coarse grains. But when the solution temperature is 545±5°C, the coarse grains of the low magnification structure begin to grow a lot.

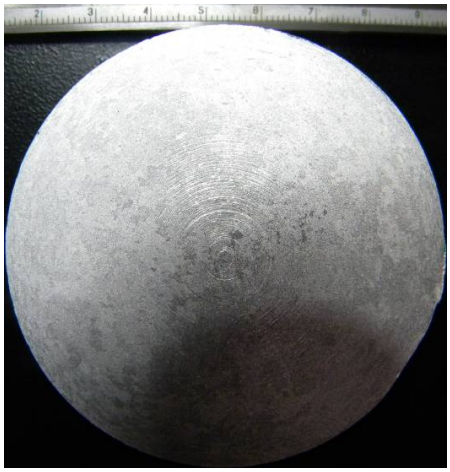

Figure 3-1 Etchant: 15% NaOH aqueous solution
Alloy and condition: 6082 alloy extruded rod
Heat treatment state: solution at 550±5℃ for 2 hours
Organization characteristics: all are coarse grains

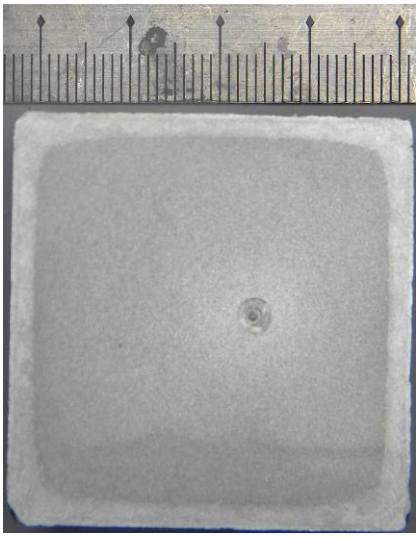

Figure 3-2 Etchant: 15% NaOH aqueous solution
Alloy and condition: 6082 alloy extruded rod
Heat treatment state: solid solution 545±5℃ for 2 hours
Microstructure features: coarse-grained rings with a thickness of 4.4 mm

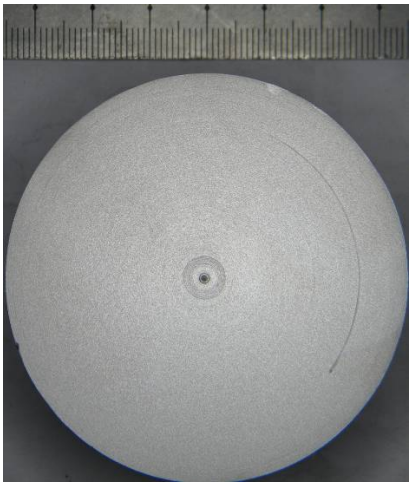

Figure 3-3 Etchant: 15% NaOH aqueous solution
Alloy and condition: 6082 alloy extruded rod
Heat treatment state: solid solution 525±5℃ for 2 hours
Microstructure: The macrostructure is uniform and the grains are small.

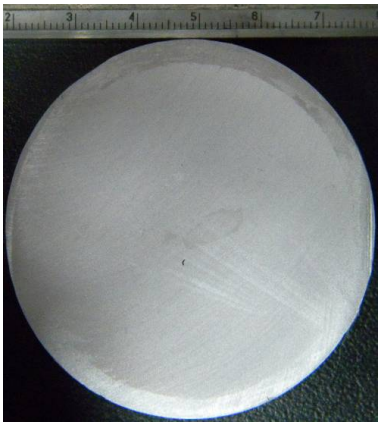

Figure 3-4 Etchant: 15% NaOH aqueous solution
Alloy and condition: 6082 alloy extruded rod
Heat treatment state: solid solution 525±5℃ for 4 hours
Microstructure: The thickness of the coarse-grained ring is 3.5mm

3.3Relationship between heat treatment temperature and high magnification structure of forged aluminum alloy 6082

3.3.1 Overview: 6082 is an aluminum-silicon-magnesium alloy that can be strengthened by heat treatment. It has high strength, heat resistance and corrosion resistance. 6082 is widely used in transportation, construction, military and civilian, and is one of the aluminum alloys with the largest output.

3.3.2 Conclusion: In order to achieve the ideal strength and hardness of the aluminum alloy that can be strengthened by heat treatment, it must be quenched to obtain a high concentration of supersaturated solid solution, and then the purpose of alloy strengthening is achieved by aging. The selection of the quenching temperature is determined according to the minimum melting temperature of the low-melting eutectic in the alloy. If the quenching temperature is too high, the material will be over-burned when it exceeds the eutectic temperature of the low-melting eutectic structure; if the quenching temperature is too low, the alloy will be overheated. The elements and the strengthening phase cannot be completely dissolved and cannot achieve the purpose of strengthening. Under the condition of not causing overburning, the higher the quenching temperature, the more complete the solid solution of alloy elements and strengthening phases in the alloy, and the higher the mechanical properties of the alloy after quenching and aging. It can be seen from the balance diagram of AL-Si-Mg alloy near the aluminum corner: the eutectic temperature of a+S+Mg_2Si is 595 ℃, and the quenching temperature of 6082 is specified as 510-590 ℃, so the 6082 alloy is the most difficult to pass through the heat treatment of the aluminum alloys that can be strengthened burnt. There are many factors that affect the overburning temperature, the main factors being the influence of alloying elements and the degree of deformation.

3.3.3 Observe and test

The working state of the 6082 alloy is used under the conditions of solid solution and aging strengthening, so this experiment did not do the process experiment in the R state. It can be seen from the figure that S decreases in a gradient with the increase of T. This is because the solid solution of the material below 595 °C is more sufficient with the increase of temperature, and the strengthening phase is more precipitated. The increase of the strengthening phase hinders the flow of the induced eddy current. Its conductivity goes down and its resistance goes up. When the temperature is above 595°C, the material has been over-burned, and the low-melting point eutectic existing in the grain and at the grain boundary is partially melted and oxidized, and the over-burned structure hinders the flow of the induced eddy current. The strengthening phase of the material is more precipitated and the strength is higher, but due to the local melting and oxidation of the low melting point eutectic in the material grain and grain boundary.

Figure 3-5 200x low-concentration mixed acid etching at 545°C (Left)

Figure 3-6 200x low-concentration mixed acid etching at 552°C(Right)

The alloy has been completely recrystallized, and the equiaxed fine-grained compounds are broken and distributed evenly, and the directional arrangement is not obvious. The alloy has been completely recrystallized, and the strengthening phases such as S phase and Mg_2Si are fully dissolved in solid solution. However, its compounds aggregate, and some grain boundaries become straight or folded. High temperature can be regarded as overheating phenomenon

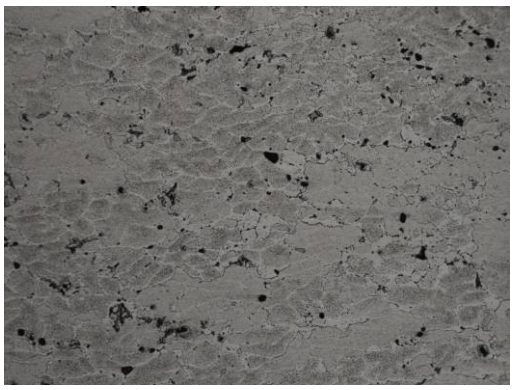

Figure 3-7 200x low concentration mixed acid etching at 592℃(Left)

Figure 3-8 200x low concentration mixed acid etching at 595℃(Right)

The heating temperature is higher and the grain size is larger, which is secondary recrystallization. The low melting point inside the grain and the eutectic form a liquid sphere, and the grain boundary is locally widened and flat, which is slightly overburned. The heating temperature is higher and the grain size is larger, which is secondary recrystallization. The low melting point eutectic inside the grain forms a liquid phase sphere, and the grain boundary is locally widened and straightened, which is an overburning phenomenon.

Figure 3-9 200x low concentration mixed acid etching at 600℃(Left)

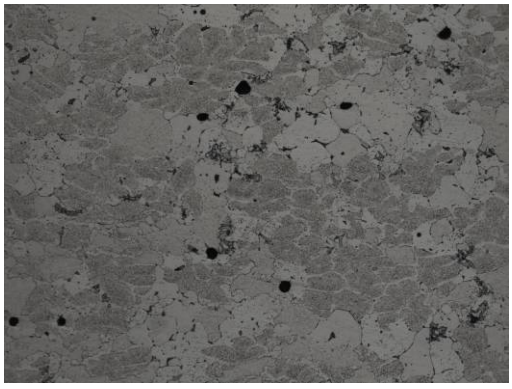

Figure 3-10 200x low concentration mixed acid etching at 605℃(Right)

Heating temperature is high. The grains are larger and are secondary recrystallization. The low melting point eutectic in the grains forms liquid spheres, and the intersection of grain boundaries is triangular, which is the phenomenon of overburning. And there are quenching cracks. The heating temperature is very high, the crystal grains are larger, which is secondary recrystallization. The low melting point eutectic inside the crystal grains forms a liquid phase sphere, the grain boundaries are widened and oxidized, and the intersections of the grain boundaries are triangular, which is a serious overburning phenomenon.

3.3.4Conclusions and Recommendations

During the heating process of the aluminum alloy, when the temperature exceeds the eutectic temperature of the low melting point eutectic structure, the local structure remelting is caused by overburning. The over-burning is mainly judged by the following three characteristics: the remelted eutectic spheres appear in the grains, the remelted local widened grain boundaries appear, and the remelted triangular structure appears at the junction of the three crystals. All the above three characteristics or their variant organization appear on the substrate, that is, the overburned organization. The above experiments show that it is reasonable to quench 6082 alloy at 500°C-590°C, and its comprehensive physical index is the most reasonable. Overheating occurs at 592°C, and overheating occurs at 595°C. In industrial production, the over-burning accident caused by human factors and equipment factors should be avoided. The inspectors should strengthen their own learning, strive to improve their professional skills, and strictly control the serious quality accident of material over-burning in the factory to ensure the quality of the manufactured products. 100 % qualified, so that users can rest assured.

Due to the limitation of equipment, only conventional analysis of materials can be performed, and deeper analysis of materials cannot be performed, such as electron microscopy, microhardness, X-ray analysis, etc.

4. Relationship between chemical composition and mechanical properties of wrought aluminum alloy 6082

4.1 Theory

The relationship between chemical composition and heat treatment of wrought aluminum alloy 6082 in Chapter 2 can be known: as the content of Si and Mg increases, the mechanical properties will also improve. As shown in Figure 4-1 and Figure 4-2

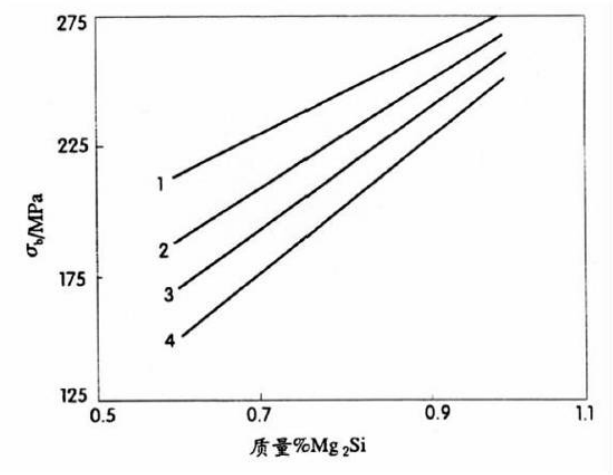

过剩量 Si 对含 0.6% ~ 1.0% Mg_2Si 合金 T6 抗拉强度的影响

1—Si 过剩量 0.25%；2—Si 过剩量 0.15%；3—Si 过剩量 0.10%；4—Si 过剩量 0.05%

Effect of Excess Si on the Tensile Strength of Alloy T_6 Containing 0.6%~1.0% Mg_2Si:1.-Si excess 0.25%; 2-Si excess 0.15%; 3-Si excess 0.10%; **4-Si excess 0.15%**

Figure 4-1 The relationship between the chemical composition range of the alloy and the tensile strength of the T6 state material

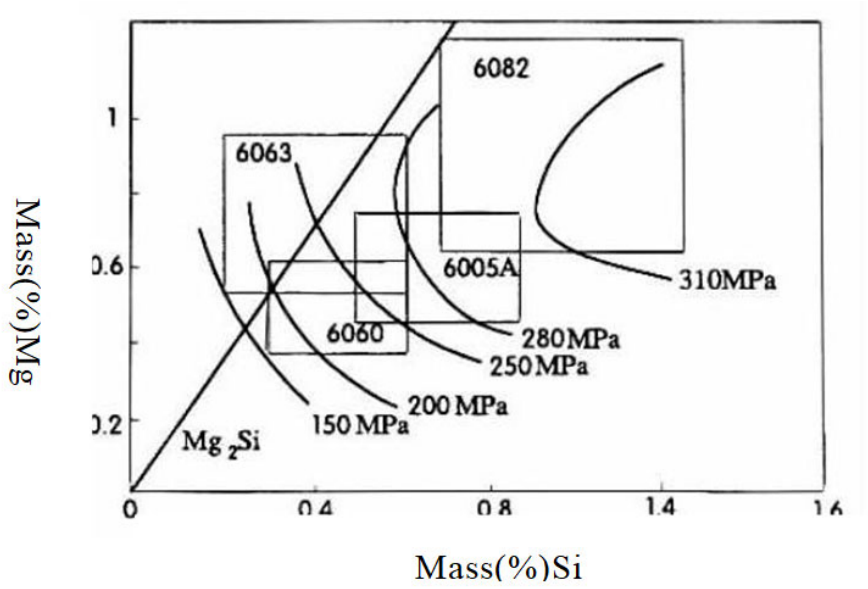

Figure 4-2 Effect of excess silicon on mechanical properties

4.2 Low chemical composition and mechanical properties

Table 4-1 Chemical composition of forged aluminum alloy 6082:

Components(%)of Element	Si	Fe	Cu	Mn	Mg	Cr	Zn	Ti
Actual(Measured) Value	1.04	0.216	0.0428	0.551	0.953	0.0939	0.013	0.0377

Heat treatment solution temperature: 545±5°C, solution time: 3 hours;
Heat treatment aging temperature: 175±5°C, aging time: 9.5 hours

The sampling location for mechanical properties analysis and the specifications of mechanical properties test bars are shown in Figure 4-3, Figure 4-4 and Table 4-2:

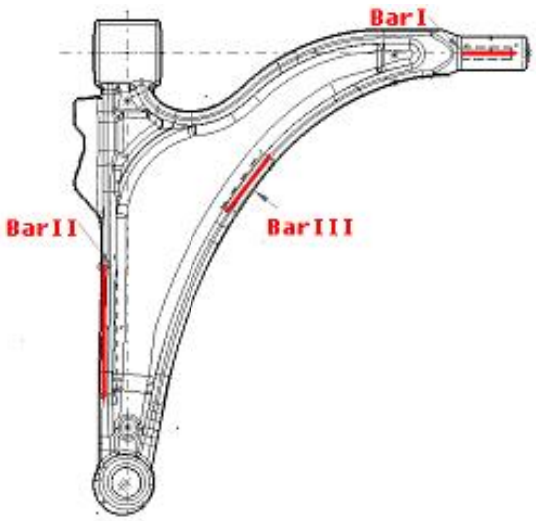

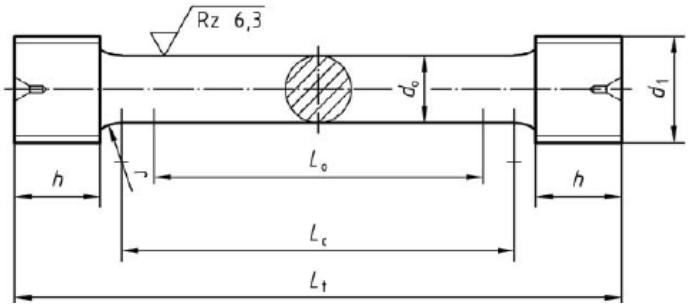

Figure 4-3 Sampling location for mechanical property analysis **Figure 4-4 Specifications of mechanical properties test bar**

Table 4-2 is the specific value of the mechanical properties test bar specifications

d_o	L_o	d_1	r min.	h min.	L_c min.	L_t min.
4	20	M6	3	6	24	41
5	25	M8	4	7	30	51
6	30	M10	5	8	36	60
8	40	M12	6	10	48	77
10	50	M16	8	12	60	97

The mechanical properties analysis data are shown in Table 4-3:

Part I: Rm average 341MPa; Rp average 309.3MPa; A (%) average 14.39
Part II: Rm average 340.62MPa; Rp average 319.9MPa; A (%) average 13.9
Part III: Rm average 355.17MPa; Rp average 326.5MPa; A (%) average 11.59

Table 4-3 Analysis data of mechanical properties of low chemical composition

NO.	编号	I			II			III		
		Rm (MPa)	Rp (MPa)	A (%)	Rm (MPa)	Rp (MPa)	A (%)	Rm (MPa)	Rp (MPa)	A (%)
1	1-1	343.83	310.544	15.706	345.45	317	17.4	349.135	322.142	14.163
2	1-2	337.041	299.753	15.864	337.3	310.5	14.6	357.781	329.345	13
3	1-8	332.211	302.892	17.885	339.4	318	12.6	354.536	334.229	9.061
4	1-14	333.363	309.41	15.102	347.605	342.169	11.391	350.448	329.582	8.5
5	1-21	337.712	301.415	14.786	334.574	307.84	15.1	358.398	328.355	13.721
6	1-28	344.5	301.276	14.052	339.8	317.84	11.75	355.515	321.043	9.667
7	2-1	344.2	310.66	16.014	346.557	322.1	10.8	357.5	327.986	10.075
8	2-11	333.754	289.76	13.248	338.4	307.2	12.9	352.94	329.739	11.2
9	2-14	368.755	334.713	16.917	355.5	339.5	14.4	355.046	329.227	12.321
10	2-15	334.307	308.17	15.172	333.1	317.3	12.3	351.067	328.657	9.174
11	2-21	342	308.8	15.1	339	308	17.5	359.898	324.705	11.881
12	2-28	345.592	313.75	15.061	338.17	337.218	14.55	355.405	322.367	8.812
13	3-1	355.571	326.068	10	346.106	326.408	14.35	353.777	320.968	14.3
14	3-4	370.566	333.291	15.4	355	325	15.5	359.858	327.783	10.063
15	3-14	331.757	306.694	18.03	339.278	312.52	14.239	354.415	319.225	11.575
16	3-15	346.768	314.068	14.256	341.3	321.3	13.8	359.354	334.384	13.737
17	3-21	334.133	304.923	18.175	331.061	306.517	13.527	353.707	318.922	11.625
18	3-28	338.28	308.5	13.335	340.383	317.667	14.695	357.092	326.291	9.508
19	4-1	344.712	312.128	12.224	349	322	14.8	353.915	329.125	9.262
20	4-12	332.179	292.721	14.337	337.9	321	16.7	357.848	322.827	16.171
21	4-14	332.081	304.588	14.234	334	318.8	15.3	359.554	336.855	13.175
22	4-15	335.41	298.785	15.623	347.8	327.6	16	352.604	327.421	11.135
23	4-21	338.707	300.771	11.804	335.009	303.459	14.276	352.497	327.395	8.451
24	4-28	330.386	306.757	13.817	339.338	319.614	11.092	359.438	328.797	10.4
25	5-1	341.36	317.487	11.856	344.3	322.9	7.873	356.097	332.198	11.76
26	5-7	340.946	334.373	12.007	340	316	17.5	356.53	323.279	15.101
27	5-14	348.895	293.996	11.175	342.3	325.7	13.277	352.965	329.826	11.437
28	5-15	340.57	310.884	14.009	336.5	319.4	10.976	353.054	323.648	10.778
29	5-21	329.833	304.161	12.926	326.958	326.5	15.7	352.648	315.436	13.541
30	5-28	340.863	317.835	13.631	337.6	319.6	12.8	352.132	323.422	14.13
Maximum	最大	370.566	334.713	18.175	355.5	342.169	17.5	359.898	336.855	16.171
Minimum	最小	329.833	289.76	10	326.958	303.459	7.873	349.135	315.436	8.451
Average	平均	341.0094	309.3058	14.392	340.62297	319.8884	13.923	355.1718	326.50597	11.591

4.3 The relationship between high chemical composition and mechanical properties

Table 4-4 Chemical composition of forged aluminum alloy 6082:

Element	Si	Fe	Cu	Mn	Mg	Cr	Zn	Ti
Actual(Measured) Value	1.23	0.2	0.0169	0.8	0.937	0.168	0.0291	0.06

Heat treatment solution temperature: 545±5°C, solution time: 3 hours;
Heat treatment aging temperature: 175±5°C, aging time: 9.5 hours

The sampling location for mechanical properties analysis and the specifications of mechanical properties test bars are shown in Figure 4-3 and Figure 4-4

The mechanical properties analysis data are shown in Table 4-5:

Part I: The average Rm is 359.6MPa; the average Rp is 328.37MPa; the average A (%) is 13.6
Part II: The average Rm is 351.994MPa; the average Rp is 329.56MPa; the average A (%) is 13.08
Part III: The average Rm is 364.39MPa; the average Rp is 335.48MPa; the average A (%) is 10.7

Table 4-5 Analysis data of mechanical properties of high chemical composition

NO.	编号	I			II			III		
		Rm (MPa)	Rp (MPa)	A (%)	Rm (MPa)	Rp (MPa)	A (%)	Rm (MPa)	Rp (MPa)	A (%)
1	L1	361.541	336.461	14.749	359.869	338.715	11.06	365.5	339.414	10.725
2	L2	357.126	324.01	14.181	349.304	323.166	14.745	363.318	343.608	10.325
3	L3	348.285	321.976	14.879	347.225	330.019	14.76	359.582	325.254	9.319
4	L4	365.654	324.89	13.218	347.61	323.312	14.679	358.073	341.78	10.4
5	L5	347.184	313.309	14.809	350.846	331.805	12.936	346.122	324.677	11.802
6	L6	351.873	318.261	13.794	347.367	313.629	12.8	372.65	331.8	9.682
7	L7	350.768	325.318	12.916	360.466	331.731	14.632	357.7	337.314	10.6
8	L8	371.429	331.817	14.622	348.454	328.619	11.283	358.182	319.06	10.01
9	L9	357.738	320.047	14.721	351.511	329.315	14.975	354.812	336.027	8.514
10	L10	350.813	311.215	12.499	349.612	336.975	12.382	345.302	329.366	12.15
11	L11	374.148	353.665	11.658	351.149	332.541	12.299	361.291	337.752	10.35
12	L12	358.023	324.823	14.181	353.042	323.166	16.049	357.589	330.532	11.05
15	L13	372.865	345.226	14.469	351.651	314.761	13.527	367.569	327.376	12.943
16	L14	390.42	376.106	13.625	354.689	323.218	13.086	364.383	330.275	12.165
17	L15	360.665	317.863	11.446	354.367	332.565	14.25	363.926	346.907	10.677
18	L16	362.48	335.566	13.084	352.773	337.596	11.174	373.575	346.409	9.2
19	L17	379.408	357.037	14.525	362.305	347.291	11.173	372.413	348.537	11.319
20	L18	361.821	339.232	12.807	355.108	337.259	13.9	366.03	338.375	10.322
21	L19	355.753	327.127	11.849	347.963	333.347	11.5	365.145	348.447	10.86
22	L20	346.766	324.838	13.992	344.711	337.08	12.5	374.634	326.456	11.187
23	L21	365.636	323.971	12.657	356.524	338.575	11.21	379.262	354.733	11.552
24	L22	362.245	338.007	13.383	354.17	336.996	10.57	371.103	344.032	11.302
25	L23	368.074	325.169	13.118	357.315	336.714	16.578	363.145	336.703	9.2
26	L24	358.318	318.33	12.778	350.345	328.875	13.542	365.241	334.589	9.021
27	L25	344.34	323.829	14.486	340.653	325.331	12.01	365.118	336.106	10.55
28	L26	353.306	329.088	12.773	351.671	327.379	15.487	365.376	337.508	12.23
29	L27	364.535	328.05	13.781	359.307	323.401	13.595	375.415	322.93	13.169
30	L28	349.34	302.83	14.125	347.003	330.779	13.025	373.873	345.412	10.541
31	L29	355.998	325.966	14.366	354.277	320.978	12.014	361.925	322.278	9.457
32	L30	343.985	318.703	14.352	341.594	303.979	10.775	354.573	325.307	10.02
33	L31	357.133	316.658	14.062	358.944	337.11	12.9	373.275	330.993	11.06
Maximum	最大	390.42	376.106	14.879	362.305	347.291	16.578	379.262	354.733	13.169
Minimum	最小	343.985	302.83	11.446	340.653	303.979	10.57	345.302	319.06	8.514
Average	平均	359.602	328.3674	13.6098	351.994	329.5557	13.0779	364.3904	335.4825	10.7

4.4 Sumary

With the above theory and data, it can be known that under the same heat treatment conditions, as well as products of the same production process, the same parts are sampled, the same type of test rods, and different chemical compositions can be obtained. With the increase of chemical composition and the ratio of rare elements Reasonable mechanical properties are improved.

5. Relationship between heat treatment temperature and mechanical properties of wrought aluminum alloy 6082

5.1 The solution temperature remains unchanged, and the aging temperature changes

1. Solid solution 560°C×0.5H, aging 180°C×2, 2.5, 3, 3.5, 4.0, 4.5, 5.0H
2. The raw material grade is 6082
3. The diameter of the raw material is 26mm
4. Heat treatment equipment: Model: RX3-15-600, working range: 50-600°C
5. Mechanical properties analysis equipment: Model: GT-TCS-2000, working range: 20000N
6. Temperature measurement method: solid temperature measurement
7. Before the test: No bubbles, scratches, etc. on the surface. After the test: no bubbles, scratches, etc. on the surface.

Table 5-1 The solution temperature is unchanged, and the aging temperature changes the mechanical property data

T(H) / Properties	2	2.5	3.0	3.5	4.0	4.5	5.0
Tensile strength (MPa)	435.527	434.872	448.897	433.923	432.132	419.183	435.435
	429.537	431.447	449.818	433.923	431.549	422.963	441.864
Yield Strength (MPa)	415.024	422.83	443.353	426.951	424.89	412.676	428.231
	412.64	420.583	444.002	426.951	425.219	416.575	435.913
Elongation （%）	12.334	11.465	10.137	10.43	10.342	10.15	10.322
	11.982	11.289	11.458	10.43	10.348	10.254	10.404

5.2 The aging temperature does not change, the solution temperature changes

1. Solution 560°C×0.5H and 570°C×0.5H, aging 180°C×3.0H
2. The material grade is 6082
3. The diameter of the raw material is 26mm
4. Heat treatment equipment: Model: RX3-15-600, working range: 50-600°C
5. Mechanical properties analysis equipment: Model: GT-TCS-2000, working range: 20000N
6. Temperature measurement method: solid temperature measurement
7. Before the test: No bubbles, scratches, etc. on the surface. After the test: no bubbles, scratches, etc. on the surface.

Table 5-2 The aging temperature remains unchanged, and the solution temperature changes the mechanical properties analysis data

Properties T(°C)	Tensile Strength（MPa）	Yield Strength（MPa）	Elongation（%）
560	448.897	443.353	10.137
	449.818	444.002	11.458
570	438.8	428.628	14.74
	432.49	423.739	13.815

5.3 Heat treatment test of semi finished product

1. Solution 570°C×0.5H, aging 180°C×3.0H
   Normal process: solution 545°C×3.0H, aging 175°C×10H
2. Material grade: cast rod 6082
3. Schematic diagram of semi finished product
4. Heat treatment equipment: Model: RX3-15-600, working range: 50-600°C
5. Mechanical properties analysis equipment: Model: GT-TCS-2000, working range: 20000N
6. Temperature measurement method: solid temperature measurement
7. Before the test: No bubbles, scratches, etc. on the surface. After the test: no bubbles, scratches, etc. on the surface.

Figure 5-1 Schematic diagram of semifinished product

Table 5-3 Analysis data of heat treatment of semifinished product mechanical properties

Properties / T(℃)		Tensile Strength （MPa）	Yield Strength （MPa）	Elongation （%）
570℃×0.5H	I	351.189	322.884	14.5
180℃×3.0H	II	353.62	323.02	12.535
	III	374.85	342.513	11.513
Normal Process:	I	356.002	334.657	13.862
545℃×3.0H	II	354.75	340.733	12.529
175℃×10.H	III	364.942	350.395	9.615

5.4 Summary

There are chapters 3 and 4, which can know that the higher the heat treatment temperature, the higher the performance of the 6082 aluminum alloy under the condition that the temperature does not exceed a certain range.

6. The relationship between low magnification structure, high magnification structure and mechanical properties of wrought aluminum alloy 6082.

6.1 Relationship between low magnification microstructure andmechanical properties of wrought aluminum alloy 6082.

6.1.1 The previous chapters 2 and 3 introduced the theoretical knowledge of low magnification structure and mechanical properties

1. Solution 545°C×3.0H, aging 175°C×10H
2. Material grade: 6082
3. Schematic diagram of semifinished product 6-1
4. Heat treatment equipment: Model: RX3-15-600, working range: 50-600°C
5. Mechanical properties analysis equipment: Model: GT-TCS-2000, working range: 20000N
6. Temperature measurement method: solid temperature measurement
7. Before the test: No bubbles, scratches, etc. on the surface. After the test: no bubbles, scratches, etc. on the surface.

Figure 6-1 Schematic diagram of semifinished product

Table 6-1 Relationship between low magnification structure and mechanical properties of blanks

NO.	Test Subject 测试项目	Spec. 测试标准	Actual Values（测量值） Bar1	Bar2	Bar3		Comments（结论）
1	Tensile strength 拉伸强度	Min340(MPa)	383.183				OK
	Yield strength 屈服强度	Min300(MPa)	356.788				OK
	Elongation 延伸率	Min10%	10.318				OK

Test Bar (DIN50125 B8*40)

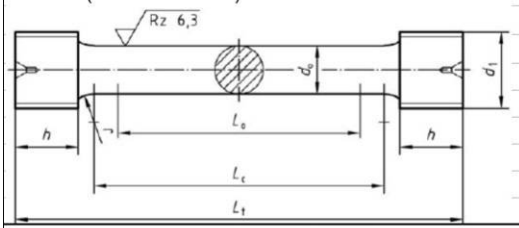

d_0	L_0	d_1	r min.	h min.	L_c min.	L_t min.
4	20	M6	3	6	24	41
5	25	M8	4	7	30	51
6	30	M10	5	8	36	60
8	40	M12	6	10	48	77
10	50	M16	8	12	60	97

Macrostructure(Cu-chloride etch)

低倍组织分析

低倍（粗晶环≤3mm）Max Recrystallized Layer 3.0mm. Around burr:8mm.

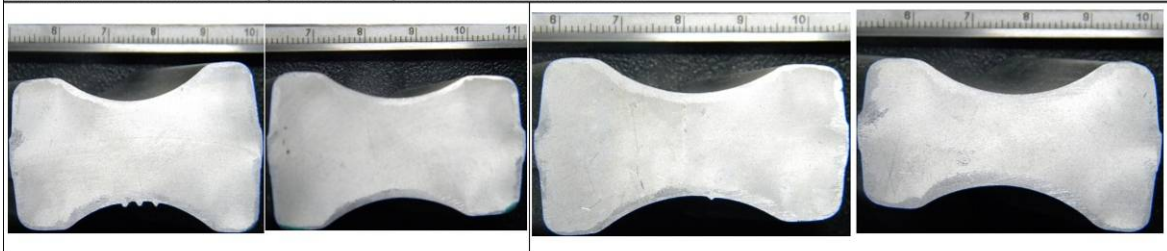

Recrystallized Layer 1.7mm, Around burr:7.2mm | Recrystallized Layer 1.7mm, Around burr:7.2mm

Test Result:Recrystallized Layer 1.7mm, Around burr:7.2mm. . It's Pass

6.1.2 Comparison of mechanical properties of coarse-grained and sub-crystalline grains on the same 6082 aluminum alloy extruded rod:

1. Solution 545℃×3.0H, aging 175℃×10H
2. Material grade: 6082
3. Material diameter is 125mm
4. Heat treatment equipment: Model: RX3-15-600, working range: 50-600^{o}C
5. Mechanical properties analysis equipment: Model: GT-TCS-2000, working range: 20000N
6. Temperature measurement method: solid temperature measurement
7. Before the test: No bubbles, scratches, etc. on the surface. After the test: no bubbles, scratches, etc. on the surface.

Figure 6-2 The thickness of the raw material coarse grain ring is 17.5mm

The mechanical properties are shown in Table 6-2:

Table 6-2 Relationship between low magnification structure and mechanical properties of raw materials

Test Subject	Spec. Standard Test	Actual(Measured) Values	
		Surface (Coarse ring site）	Central（subcrystalline）
Tensile strength	Min350(MPa)	346.63	399.3
Yield strength	Min310(MPa)	313.577	372.95
Elongation	Min10%	18.48	13.8

6.1.3 Summary

From the above, it can be known that the relationship between mechanical properties and low magnification structure is that the mechanical properties without coarse grains are the best, but the mechanical properties decrease within a certain range with the increase of coarse grains.

6.2 Relationship between high magnification microstructure and mechanical properties of wrought aluminum alloy 6082.

6.2.1 Specimen: a high-magnification sample for forging raw materials in 6082H112 state, and a high-magnification sample in 6082T6 state after forging. The raw material for macroscopic observation is extruded material.

6.2.2 Test: 1. Grind the transverse section in the main deformation direction of the raw material to a high magnification, see Figures 6-3, 6-4, 6-5.

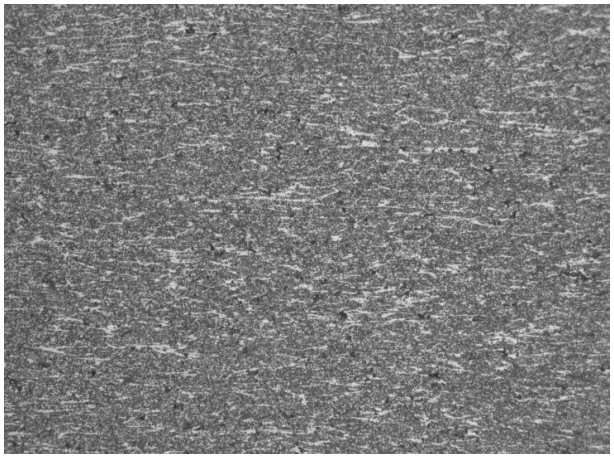

Figure 6-3 6082H112-1 200X

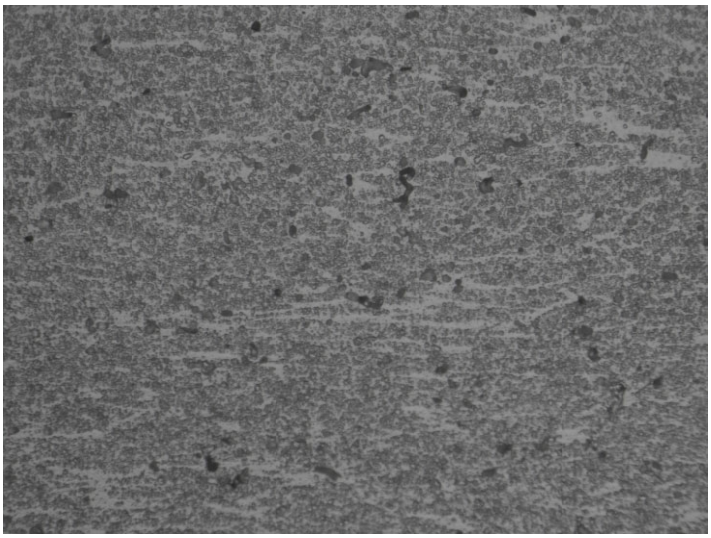

Figure 6-4 6082 H112-1 500X

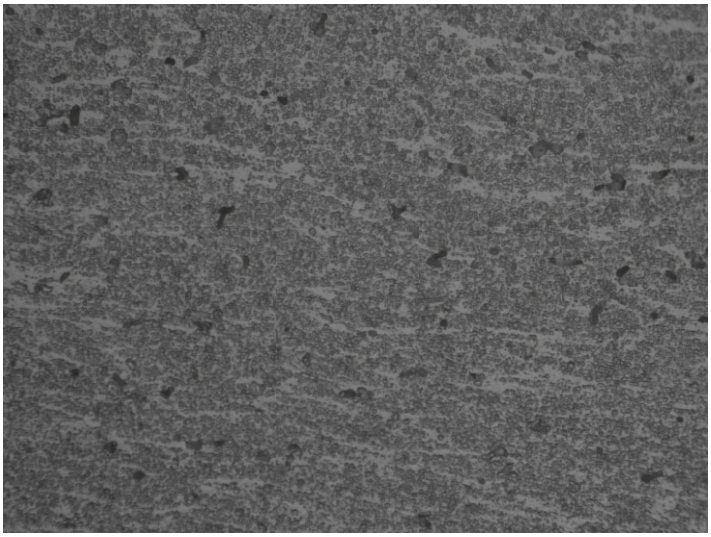

Figure 6-5 6082 H112-1 500X

2 After forging, the transverse section of the main deformation direction of the material is ground to a high magnification, as shown in Figures 6-6, 6-7, 6-8.

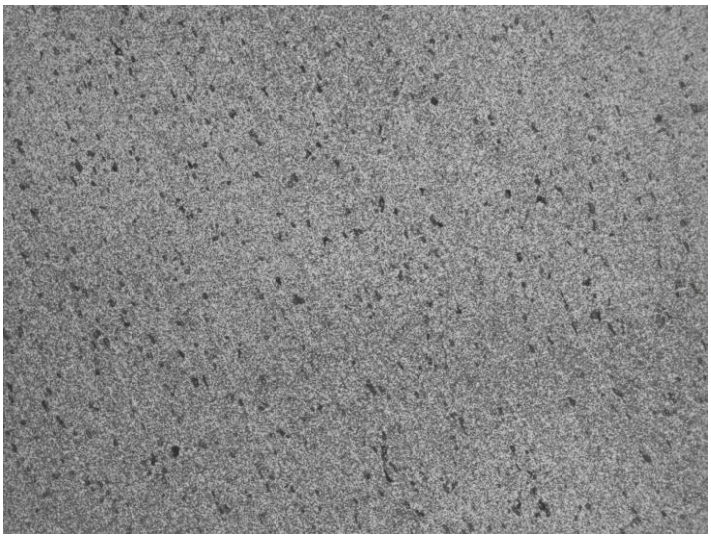

Figure 6-6 6082T6-1 200X

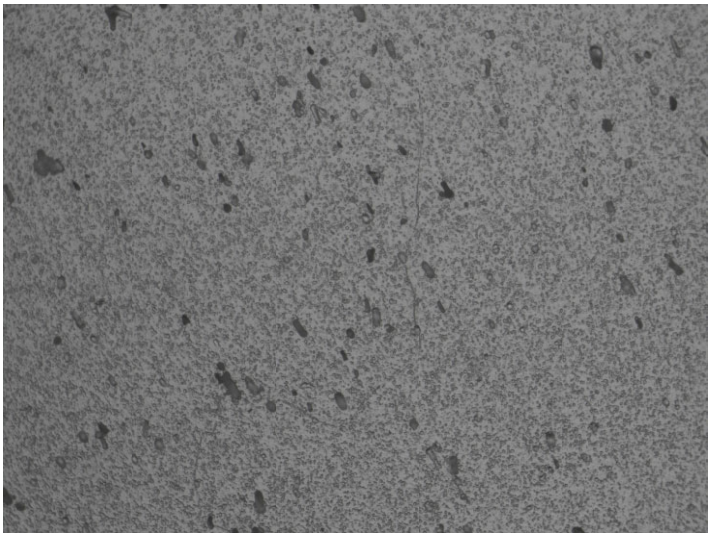

Figure 6-7 6082T6-1 500X

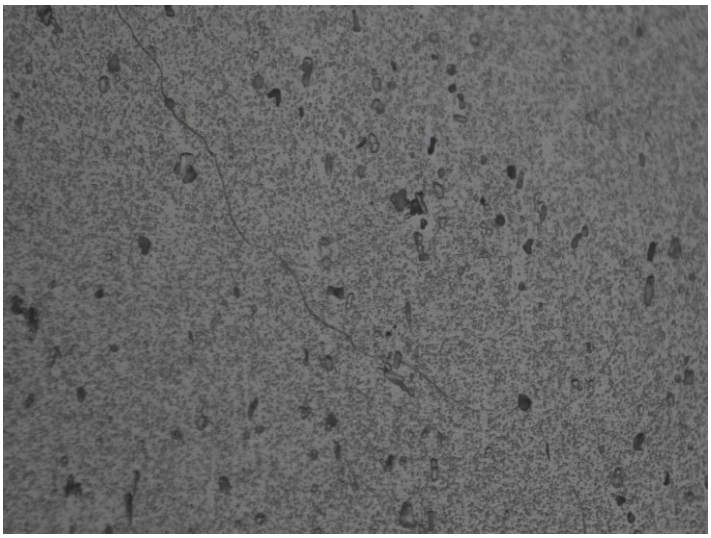

Figure 6-8 6082T6-1 500X

6.2.3 High magnification tissue analysis:

1. The raw material is observed under an optical microscope at a high magnification: the material has been completely recrystallized, equiaxed, the compound is sufficiently broken, and the structure is uniformly distributed along the extrusion direction, but the solid solution is insufficient.

2. Macroscopic observation of the sample after forging: the grains are coarse and the grain distribution is anisotropic, which is related to the design of the forging die and the forging process; observed under an optical microscope, the material has been completely recrystallized, the grains are coarse, and the compound is fully broken. The strengthening phase is dispersed and precipitated, the grain boundaries are slender, the grain boundaries are not widened, there is no remelting eutectic sphere, there is no triangular grain boundary, the forging deformation is sufficient, the grains are coarse, but the solid solution is sufficient.

6.2.4 Mechanical property analysis

Bar 2 and Bar 3 are 6082 H112 condition bars and Bar 1 is 6082 T6 condition bars

Table 6-3 Mechanical property data of H112 and T6

Test Subject	Spec. Standard Test	Actual(Measured) Values		
		Bar1	Bar2	Bar3
Tensile strength	Min350(MPa)	390.796	186.05	184.53
Yield strength	Min310(MPa)	369.362	164.824	156.37
Elongation	Min10%	13.3	7.19	8.14

Therefore, the mechanical properties will increase with high solid solution and sufficient performance, and decrease with coarse grains, and so on.

7. The relationship between chemical composition and low magnification tissue and high magnification tissue

From the analysis of theoretical knowledge in chapters 2 and 3, it can be known that the relationship between the chemical composition of 6082 aluminum alloy and the low-magnification structure and high-magnification structure is as follows: A certain amount of Fe and titanium can be added to the composition to eliminate. 6082 is prone to coarse columnar crystals during casting and solidification, especially when the iron content is low. Figure 7-1 The cylindrical rod of 6082 alloy DC casting has the problem of partial fine grains (columnar grains) due to the difficulty of grain refinement. If there are many solute elements in the alloy, the problem of solidification to produce coarse grains (columnar grains) is less, but purer aluminum alloys or commercial pure aluminum are prone to produce equiaxed and columnar grains in the casting process. The two structures are mixed as shown in the figure 7-2. Figure 7-2(a) shows that the position close to the mold wall solidifies to form equiaxed crystals, but the subsurface to the center produces directional columnar crystals, and finally the central position (in the last solidified region) produces equiaxed crystals. Figure 7-2(b) shows the solidified structure of 6082 cast DC without the use of an effective refiner.

If the grain structure of casting solidification is to be completely refined and equiaxed as shown in Figure 7-2(a), a refiner such as AlTiB master alloy needs to be used during casting to refine the grains. In addition to the appropriate amount of addition for effective solidification and refinement, the distribution of the refiner in the solidified aluminum liquid should also be uniform. As shown in Figure 7-3, 6082 aluminum DC casting can use effective refiners such as TiB_2 or $AlTi_3$ particles to make columnar grains disappear into equiaxed fine grains. Basically, the effective refiner is the nucleus where the grain begins to solidify. The nucleus grows during the solidification process and finally becomes a dendrite. The interface between the nucleus and the nucleus with a dendrite after solidification is regarded as the grain boundary. Basically a dendritic crystal. Therefore, the number of effective refiners determines the size of the grains. The more effective refiners are, the finer the solidified grains are. But the added refiners are not all effective,

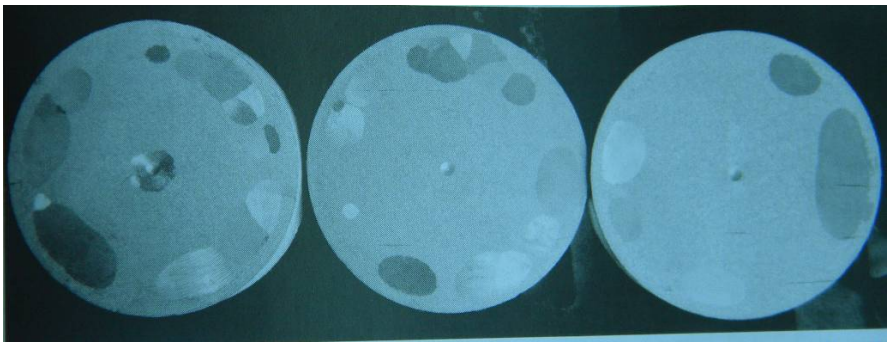

Figure 7-1 6082 alloy D38mm cast rod: equiaxed grain and columnar coarse grain (incomplete grain refinement)

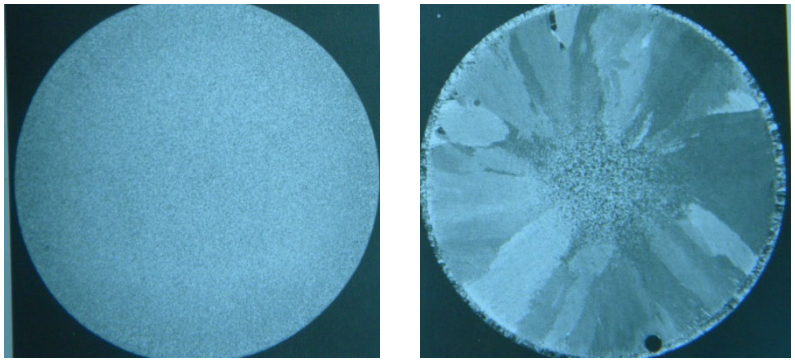

Figure 7-2 6082 alloy DC casting a) with refiner, b) without refiner

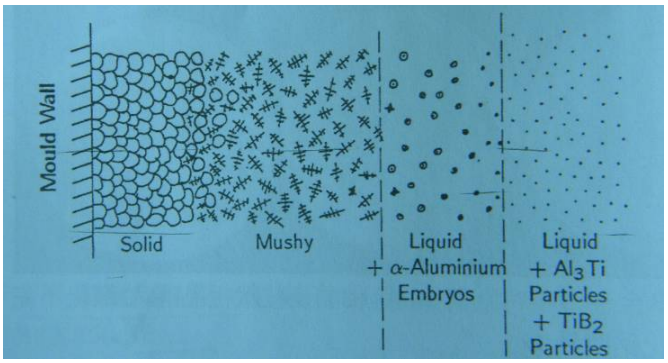

Figure 7-3 6082 alloy DC casting uses effective refiner to make columnar grains disappear into equiaxed fine grains
(Photo courtesy of Lennart Backerud, Ella Krol and Jarmo Tamminen)

In addition to the mixture of equiaxed crystals and columnar crystals, the non-uniform solidified structure is commonly a mixture of floating crystals and dendritic crystals produced during the casting process. The products produced by the mixture of two different structures can be clearly displayed after anodic surface treatment. Like the above columnar crystal defects, if the ingot is used for processing, it is unacceptable. The product of 6082 shown in Figure 7-4. From the metallographic observation, the floating crystal is similar to the grain shape after plastic working, but there is no solidification redistribution of the solute, and it is also a huge segregation during the solidification process. Because it is different in composition from dendrites, there is no way to process and heat it to remove it.

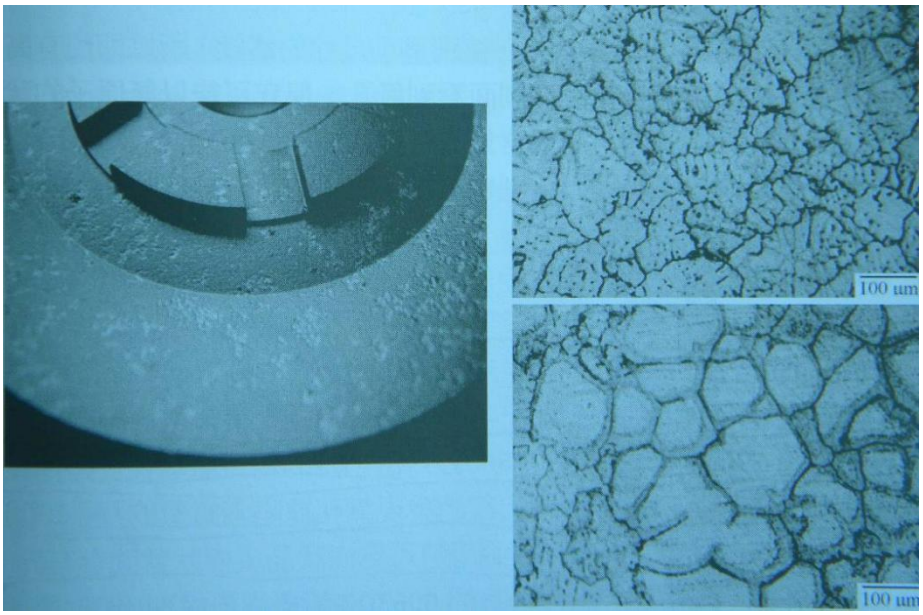

Figure 7-4 6082 floating crystal produces bright spots on the anode (left picture), and metallographic analysis contains dendrites (top right picture) and floating crystals (bottom right picture)

Uneven chemical composition will cause low-fold segregation of products, and some elements in the chemical composition are too low to appear various feathery crystals, bright crystals and other depressions. The following low magnification segregation is an example: as shown in Figure 7-5, 7-6, 7-7

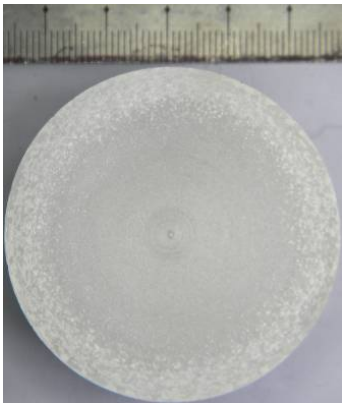

Figure 7-5 Segregation, the thickness of the segregation is 7.8mm

Figure 7-6 All coarse grains

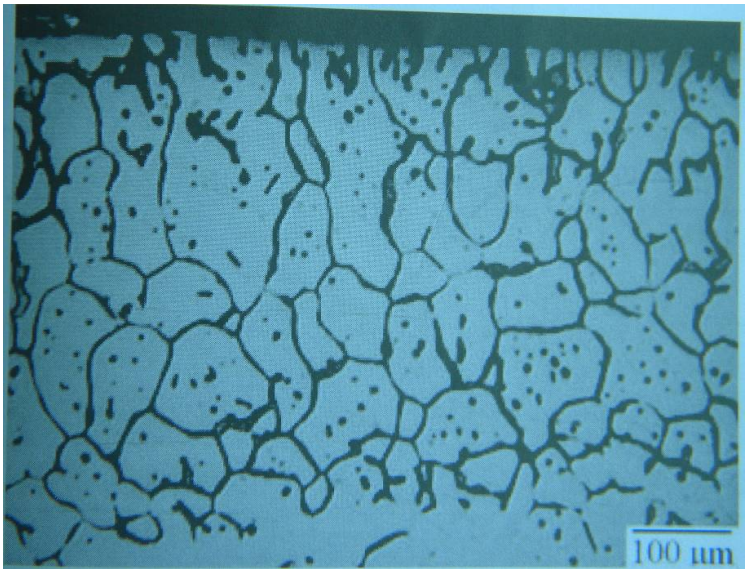

Figure 7-7 6082 alloy, the metallographic structure of the segregation layer (Keller corrosion)

8. Effect of Quenching Cooling Rate on Mechanical Properties of 6082 Aluminum Alloy

8.1 Introduction of quenching processon mechanical properties of 6082Al

Alloy 6082 is a typical heat-treatable reinforced aluminum alloy with moderate strength and good weldability, formability and corrosion resistance. It is often used as civil profiles (such as building materials) and in the manufacture of various structural parts, such as high-speed trains and hull structural parts. et al [6, 7, 8]. Quenching the 6082 alloy at a very high cooling rate can reserve more vacancies and solute atoms, but an excessively high cooling rate will produce uneven residual stress; while an excessively low cooling rate will cause the solid solution to decompose and the vacancy density will decrease, so that the alloy The solute atoms in the matrix are preferentially nucleated and grown on the grain boundaries or dispersed phase particles, which consumes a large amount of solute atoms and vacancies in the matrix and weakens the aging strengthening. Both too high and too low cooling rates will reduce the mechanical properties of Al-Mg-Si alloys [9,10,11]. The trace elements Sc[12] and aging[13] have different effects on the quenching sensitivity of alloys, however, the quenching sensitivity of heat-treatable alloys depends to a large extent on the quenching precipitation behavior at different cooling rates [14] .

B.C. Shang used the TTP curve to study the quenching sensitivity and transformation kinetics of 6082 alloy [15], and obtained the quenching sensitivity of the alloy according to the quenching factor k, the critical temperature range and the critical cooling rate. This method is more complicated, and the end quenching method is relatively simple. The end-quench experiment(also called 'Jominy end-quench test') was originally designed to determine the hardenability of steel. Deng [16] et al evaluated the hardenability of many Al-Zn-Mg-Cu alloys by this method, Yu-Chih Tzeng[12] et al gauged the hardenability of Al-7Si-0.6Mg-0.04Sc alloy by JEQ test The penetration depth is about 60 mm, and Tian N [17] et al. obtained the critical cooling rate at different positions from the quenched end during extrusion using end quenching experiments. This shows that the hardenability of heat-treatable-enhanced aluminum alloys acquired by the JEQ test is of great meaning for determining the quenching process of the alloys. In this paper, end quenching of 6082 aluminum alloy was carried out and combined with JMatpro7.0 software simulation to study the effect of quenching rate on quenching sensitivity and the relationship between mechanical properties and microstructure of the alloy under different cooling rates.

8.2 Experimental method

The diameter of the 6082 aluminum alloy extruded bar used in the experiment is 30 mm and the length is 130 mm, and its chemical composition is listed in Table 8.1.

Table 8.1. Chemical composition of 6082 aluminum alloy used in the experiment (mass fraction, %)

Components of the Sample	Mg	Si	Cu	Fe	Mn	Cr	Zn	Ti	Al
Actual(Measured) Value	0.97	1.20	0.01	0.22	0.87	0.18	0.02	0.04	Bal

The samples were solution-treated at 530 °C/1 h in a salt bath furnace, and then shifted to the end-quenching device (CK-III-2) at once for end-quenching experiments. The samples were free-end quenched in water at 20 °C for 10 min. The end-quenched samples were cut along the center line and immediately subjected to aging treatment at 180 °C for 5 h. Figure 8.1(a) shows the schematic diagram of the end quenching device, and 1b shows the quenched sample. Thermocouples with a diameter of 1.5 mm were inserted at 5 mm, 20 mm, 40 mm, 70 mm, and 120 mm from the quenching end and connected to a temperature controller to record the temperature changes at different positions during the quenching process. The MHBS-3000 digital Brinell hardness

tester was used to measure the hardness of the samples after aging, starting from D=5 mm from the quenching end, and testing the hardness every 8 mm, with a loading load of 250 kgf and a loading time of half a minute. Samples with dimensions of 12 mm × 8 mm × 1 mm (perpendicular to the extrusion direction) were taken at distances D=1 mm, 20 mm, and 70 mm from the quenching end for microstructure observation. The tissue of the samples was observed with a TECNAI G2 F20 transmission electron microscope with a loading voltage of 200 KV. Preparation of transmission samples: first grind the samples to 80 um with sandpaper, punch holes to obtain discs with a diameter of 3 mm, and then perform electrolytic double-spray thinning. -30℃ or less. The width of grain boundary PFZ was measured using Nano Measure software, and the average of 10 measurements was taken.

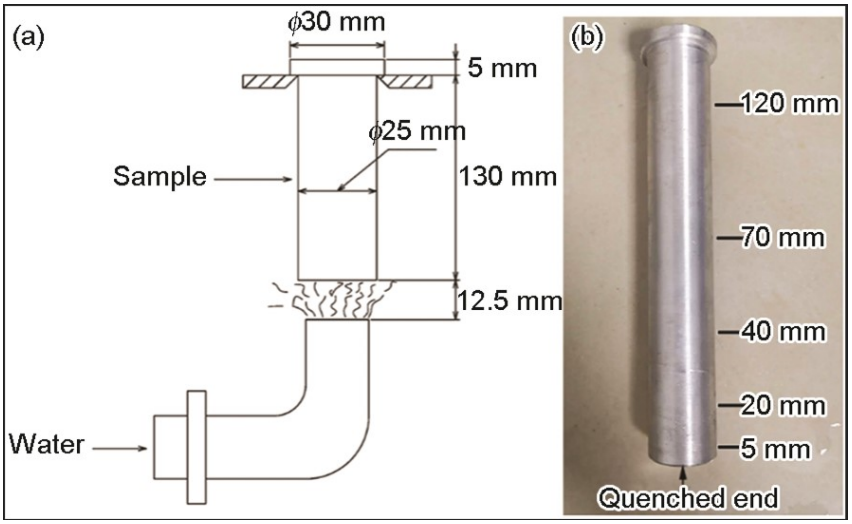

Fig.8.1 Schematic diagram of end quenching device:(a)and end quenching sample(b)

8.3 Results

8.3.1 TTT curve and CCT curve of 6082 alloy

JMatpro7.0 is a thermodynamic calculation software for calculation and performance simulation based on the phase diagram of metal materials [18], based on the thermodynamics and kinetics of phase transition. The transformation fractions of every phase at discrepant temperatures and times are computed and recorded in the coordinate system of isothermal treatment temperature and time, so as to gain the TTT curve and CCT curve of the alloy.

The TTT curve and CCT curve of 6082 alloy are both "C" type, the TTT curve in Figure 8.2(a) shows that the peak temperature of β', β" phase is 375 ℃, at this temperature the β', β" phase is easy to disengage. Dissolution and precipitation; the nose tip temperature of β phase is 425 °C, and the β phase is directly desolubilized and precipitated from the solid solution around this temperature. Figure 8.2(a) also shows that the alloy has a quenching sensitive range of 220–425 °C. In this temperature range, the supersaturated solid solution of the alloy has a high decomposition rate and a short incubation period. The CCT curves simulated by JMatpro7.0 software show that in order to inhibit the precipitation of β' (metastable phase) during the quenching process, the critical quenching cooling rate of the alloy must be greater than 6°C/s (Fig. 2b).

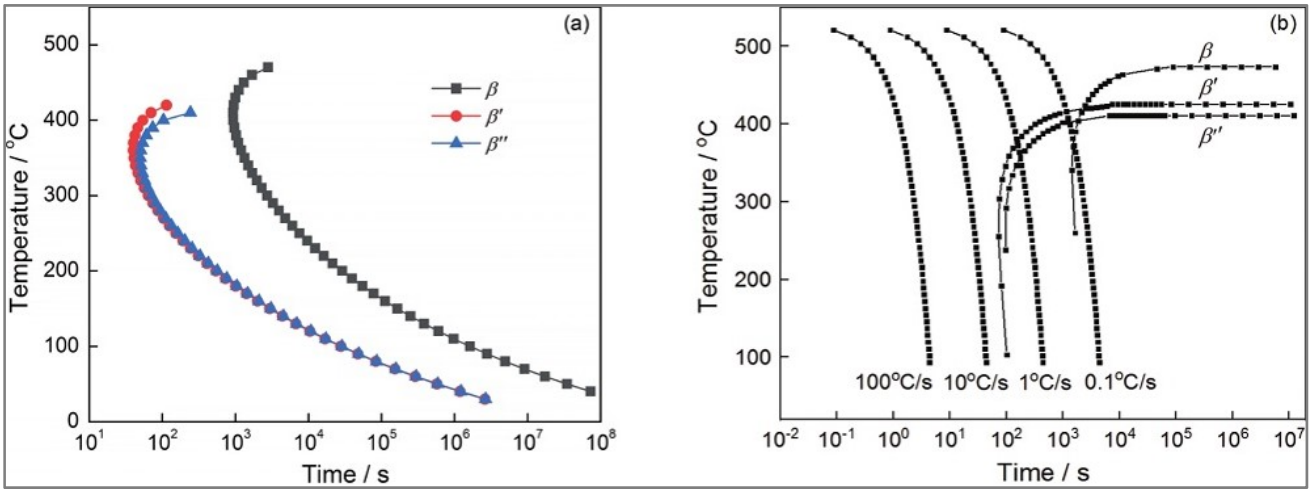

Fig.8.2 TTT curve (a) and CCT curve (b) of 6082 alloy simulated by JMatPro 7.0 software

8.3.2 End Quenching Cooling Curves and Average Cooling Rates at Different Locations

Figure 8.3(a) shows the end quenching cooling curves at 5 mm, 20 mm, 40 mm, 70 mm, and 120 mm from the quenching end. The temperature drops sharply from 530 to 150 °C, and slowly decreases from 150 °C to room temperature. It can be seen from Fig. 8.3(b) that the average cooling rate of the alloy decreases with the increase of the end quenching distance D, and the decrease is the fastest between D = 5 mm and D = 30 mm. The average cooling rate at D=5 mm reaches a maximum of 44.07°C/s, and the average cooling rates at D=20, 40, 70, and 120 mm are 8.24, 2.47, 1.84, and 1.74°C/s, respectively. The relationship between the quenching rate v and the end of the quenching distance D is

$$v = 1.72 + \frac{44.89}{1+(D/11.71)^{3.31}} \quad (1)$$

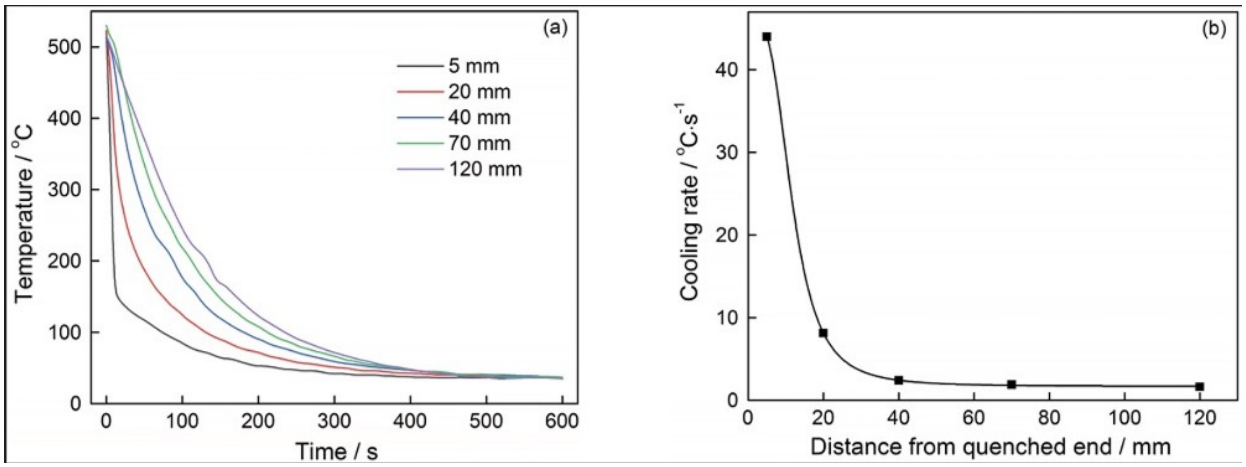

Fig.8.3 End quenching cooling curve(a)and average cooling rate(b) at different locations

8.3.3Mechanical properties of aged alloys

The curve of hardness distribution for the end-quenched specimen in the aging state is shown in Fig. 8.4(a). It can be seen that the hardness curve of the alloy shows a continuous downward trend with the increase of the end quenching distance D, and the hardness reaches the maximum value of 97.8 HB at D=5 mm. Define Hardness Loss Values

$$\mathrm{R} = \frac{\mathrm{Hardness_{5mm}} - \mathrm{Hardness_{xmm}}}{\mathrm{Hardness_{5mm}}} \times 100\% \quad (2)$$

The hardenability of 6082 aluminum alloy is quantitatively characterized, where $\mathrm{Hardness_{5mm}}$ is the hardness value corresponding to the distance D=5 mm from the quenching end, and $\mathrm{Hardness_{xmm}}$ is the hardness value corresponding to the distance D=Xmm from the quenching end. The position corresponding to R=10% is defined as the hardening depth of the alloy [19], and the hardening depth of 6082 aluminum alloy is 23 mm. It can be known from formula (1) that the corresponding quenching rate here is 6.07°C/s.

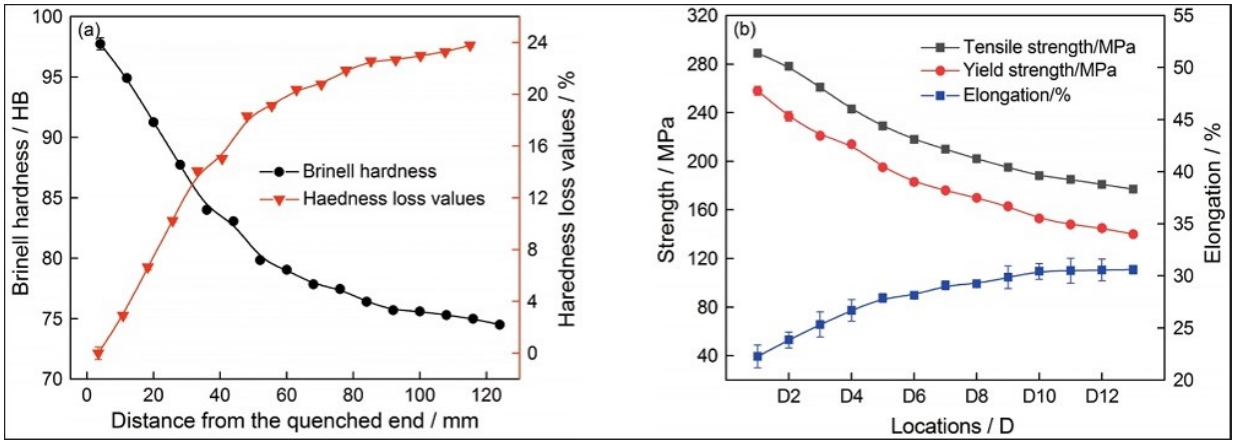

Fig.8.4 Hardness curves and hardness loss values of aged JEQ bars(a)and drawing curves of tensile results at different positions(b)

Cut the aging JEQ bar into 13 segments, numbered D_1, D_2..., D_{13}, and take the center position of each segment for tensile property testing. Figure 8.4(b) presents the curve drawn from the tensile results of the JEQ rod. It can be seen that the yield strength and tensile strength of the alloy decrease with the enlargement of quenching distance D. The tensile strength, yield strength and elongation at D_1 are 289 MPa, 258 MPa, and 22.3%, respectively; The tensile strength, yield strength and elongation are 177 MPa,

140 MPa, and 30.6%, respectively. It can be seen from Figure 8.4(b) that the strength decreases the fastest from D_1 to D_5, and the elongation increases the fastest. The strength decreases slowly from D_6 to D_{13}, and the elongation remains basically unchanged. The comprehensive properties of the material under rapid quenching are better.

8.3.4 Microstructure of as-quenched 6082 alloy

8.3.4.1 TEM morphology of the alloy as quenched

Figure 8.5 shows the TEM morphology of the alloy as quenched, and the incident direction of the electron beam is the [001]Al direction. Figure 8.5 shows that there is no quenched precipitate at the grain boundary and intragranular of the alloy at D=1 mm, but some micron-scale gray-black phases appear in the grain. These gray-black phases are Mn-containing α-(AlMnFeSi) phases [20, 21, 22] generated during the homogenization process, which have high thermal stability, as shown in Figures 8.5(a) and 8.5(d). At D=20 mm, the lamellar phase precipitates on the gray-black phase, and the energy spectrum analysis results show that it is the β phase. Figure 8.5(c) shows the morphology of the end-quenched sample at D=70 mm. It can be seen that the precipitates on the α-(AlMnFeSi) dispersion grow along the length direction, and the length is about 300 nm. From Fig. 8.5(e), it can be observed that there is a small amount of quenched precipitates at the grain boundaries. During the end quenching process, when the quenching rate is low, the quenched precipitates are easy to nucleate and precipitate on the grain boundaries and the Fe and Mn-rich phase particles.

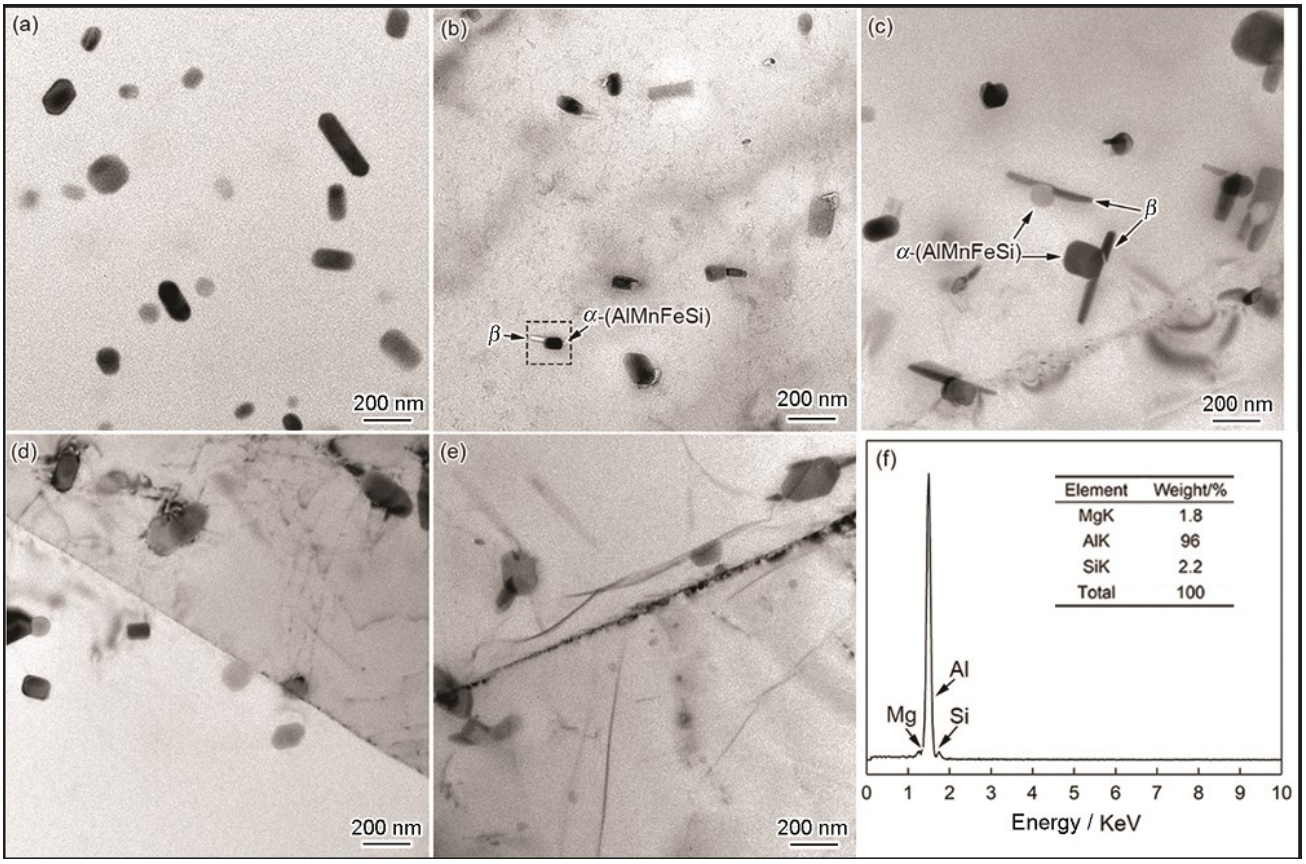

Fig.8.5 TEM morphology of quenched 6082 alloy: (a), (d) D=1 mm; (b) D=20 mm; (c), (e), (f) D=70 mm

8.3.4.2 TEM morphologies of aged alloys

Figure 8.6 indicates the TEM morphologies of the alloys aged at 180 °C for 5 h at discrepant positions from the quenching end. At D=1 mm from the quenching end (the quenching cooling rate is 46.59℃/s), in the rapidly quenched sample, it can be observed in Fig.8.6(a). It is about 3~4 nm and the length is about 10~30 nm, and it is precipitated along the [100]Al and [010]Al directions. A large number of granular precipitates can also be observed in Fig.8.6(a), with a diameter of about 2–3 nm. These precipitates are GP zone structures or cross-sections of intercalated needle-shaped precipitates. It could be noticed from the corresponding electron diffraction pattern (SAED) in Fig.8.6(d) that a very weak "cross" pattern appears near the [110]Al under the [100]Al crystal band axis. As the main precipitation phase in Al-Mg-Si alloy, β" phase has a good strengthening effect. At D=20 mm from the quenching end (the quenching cooling rate is 8.25℃/s), the needle-like precipitates in the alloy grains decrease. At D=70 mm from the quenching end (the quenching cooling rate is 1.81 °C/s), as shown in Figure 8.6(c), the needle-like precipitates β" in the crystals are significantly reduced, and rod-like precipitates β' appear, with a diameter of about 5~10 nm. , with a length of 80–100 nm. Since β' maintains a semi-coherent relationship with the matrix and has a degree of mismatch with the matrix, it forms a certain strain field with the matrix [23,24], which makes the "cross" pattern of the electron diffraction pattern in Fig. 8.6(f) remarkable. enhanced.

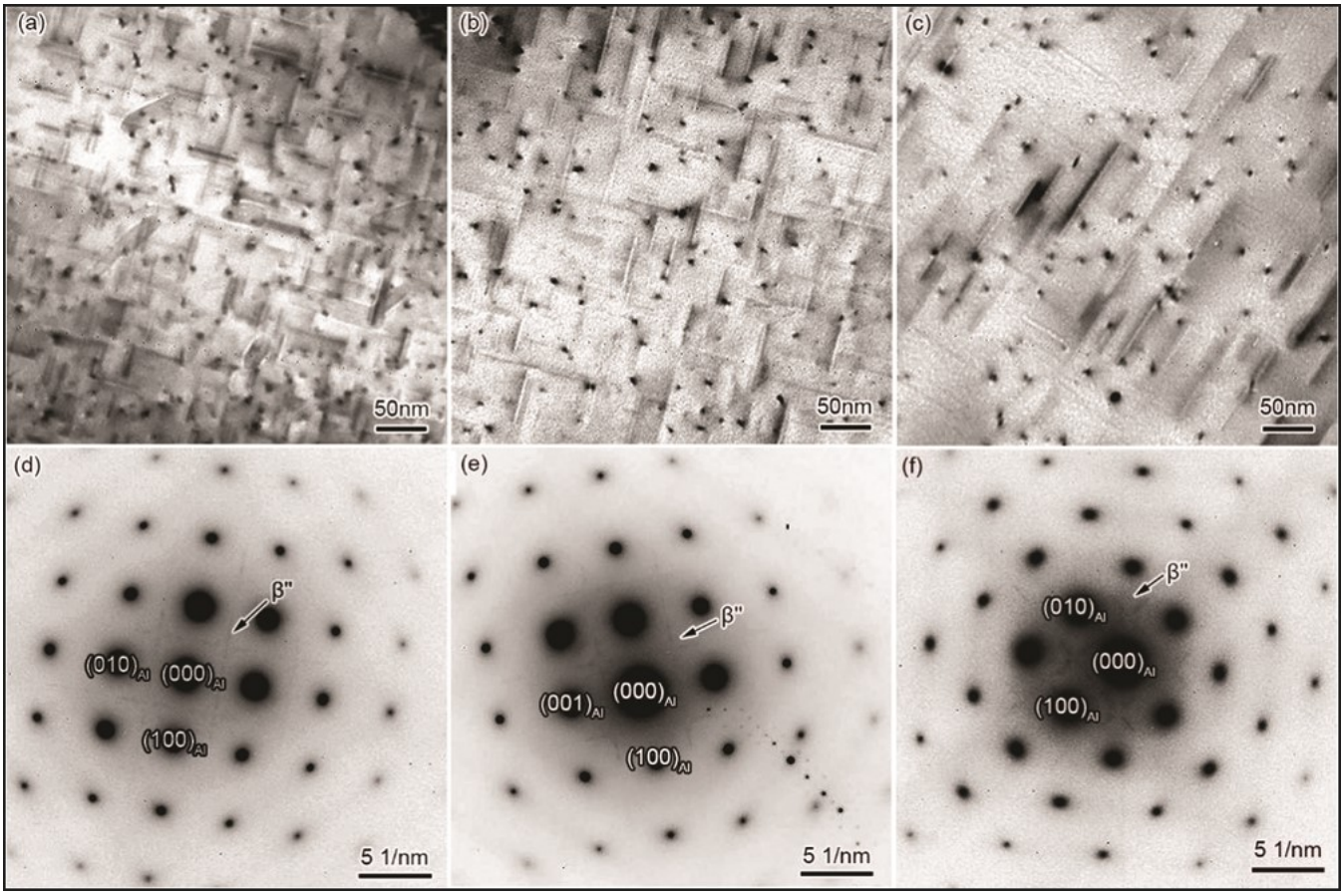

Fig.8.6 TEM morphology of aged 6082 alloy：(a), (d) D=1 mm; (b), (d) D=20 mm; (c), (f) D=70 mm

Figure 8.7 presents the TEM morphologies of the alloys at the grain boundaries in the aged state. It can be observed that when the quenching cooling rate is large, that is, when the cooling rate is 46.59 °C/s at D=1 mm, a small amount of fine β equilibrium phase precipitates on the grain boundary and is continuously distributed, and the grain boundary does not appear at this time. Obvious PFZ; at D=20 mm from the quenching end, the quenching cooling rate is 8.25℃/s, and obvious PFZ appears at the grain boundary, and the PFZ width at this time is (157±2) nm; at D=70 mm, when quenching When the cooling rate is as low as 1.84°C/s, a wider PFZ appears in Fig. 8.6(c), the equilibrium on the grain boundary is coarser than that at D = 1 mm, and the distribution is discontinuous, and the width of the PFZ at the grain boundary reaches (226±2) nm .

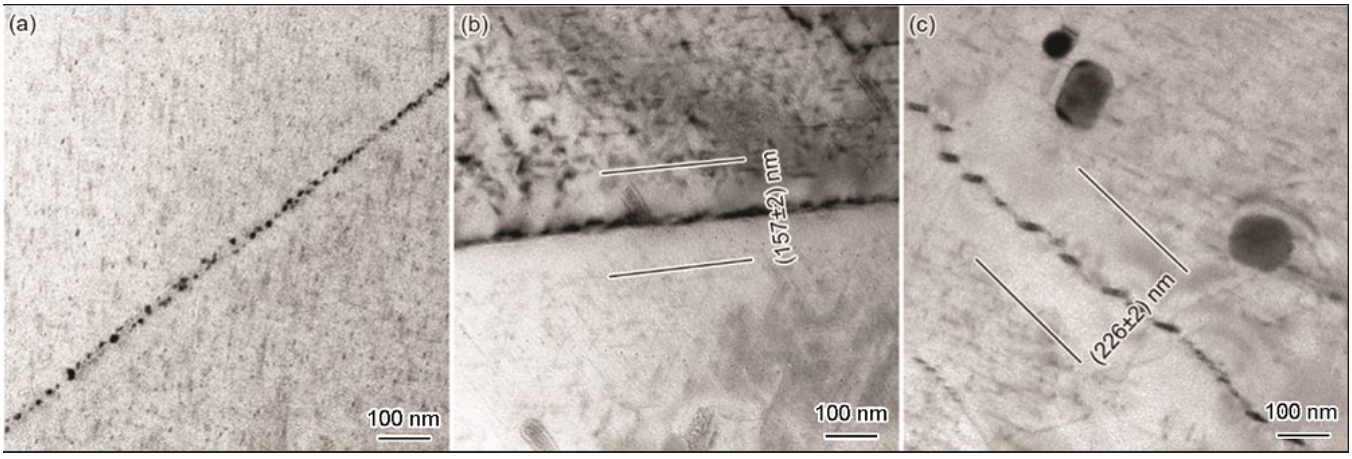

Fig.8.7 TEM morphology of grain boundaries of 6082 alloy as aged:(a) D=1 mm; (b) D=20 mm; (c) D=70 mm

Figure 8.8 shows the intragranular morphology of the alloy in the aging state. Figures8.8(a) and 8.8(b) are the micro-morphologies at low magnifications, and Figures 8.8(c) and (d) are the enlarged morphology of the black box. Comparing Figure 8.8(c) and (d), it can be seen that when the quenching cooling rate is as low as 2 °C/s, the β" precipitation strengthening phase near the quenching-induced precipitation phase β is significantly reduced, and a PFZ region with a diameter of about 400 nm appears around.

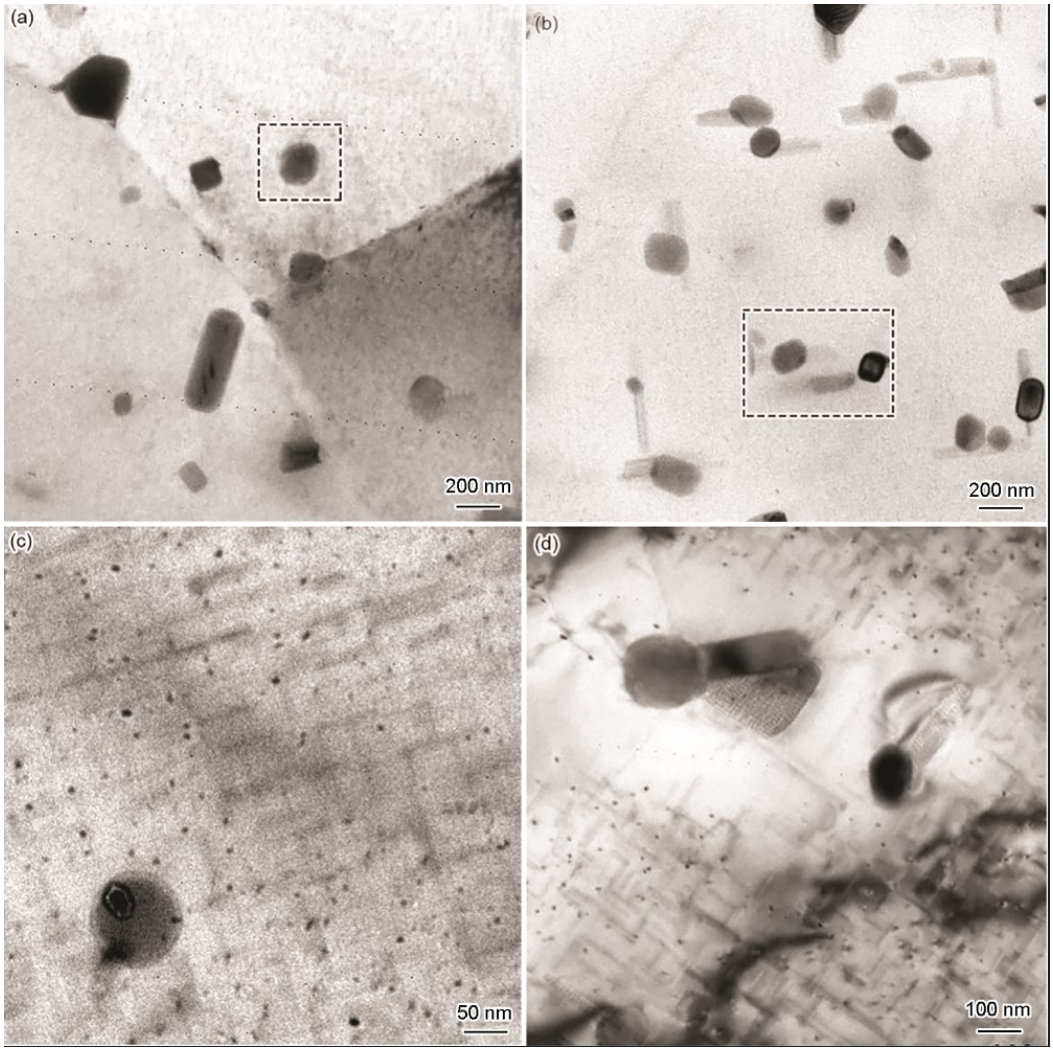

Fig.8.8 TEM morphology of aged 6082 alloy intragranular (a), (c) D=1 mm; (b), (d) D=70 mm

8.4 Analysis and Discussion\

8.4.1Precipitation kinetics of quenching-induced precipitates

The end quench test can simulate the flow of heat from the center to the surface of the thick plate in one dimension, so the quench cooling rate varies with the location of the quench end, with the greatest difference in cooling rate at both ends of the rod, as shown in Figure 8.3. The quenching sensitivity is determined by the alloying element concentration and nucleation position, so the nucleation rate of the precipitated phase in the final quenching process in this experiment is [19]

$$I = c_1 \times exp[-\frac{\Delta G^* + Q}{KT}] \qquad (3)$$

where c_1 is a constant, ΔG* is the nucleation work (J), Q is the diffusion activation energy (J) of the solute atom (which changes little with temperature), which can be approximated as a constant, and K is the Boltzmann constant (J/k), T is the absolute temperature (K). ΔG* is closely related to the degree of subcooling. Super cooling can provide more power to drive nucleation when the temperature declines to a definite range (220~425°C in this study). Simultaneously, the temperature-controlled diffusion process will affect the subsequent coarsening of the β-equilibrium phase (Fig. 8.5(b) and (c)).

In the higher temperature range (T>425°C), the diffusion of solute atoms is very fast, however, the driving force of the phase transition is not large enough, so the nucleation rate is not high. In the lower temperature range (T<220°C), the coarse equilibrium phase is rarely precipitated owing to the low diffusion rate of solute atoms. In the middle temperature range (T=220~425°C) are the diffusion rate and driving force of solute atoms relatively large (such as Equation 3), and the quenching sensitivity of the alloy is the highest. Therefore, proper diffusion rate and nucleation activation energy are necessary conditions for phase transition within a definite temperature range. Additionally, the time of phase transition is also a significant factor. The phase transition takes longer at high or low temperatures compared to the mid-temperature range. In the end quenching experiment, the time required for cooling from 530 °C to room temperature was different at different positions from the quenched end of the sample (Fig. 8.3(a)). It can be seen from Figure 8.3(a) that the quenching cooling rate at D=1 mm from the quenching end is 46.59 °C/s. At this time, the driving force is very large, but the time for atomic diffusion is limited. Therefore, the coarse quenching equilibrium phase is not observed in Fig.8.5(a). However, in the parts D=20 mm and D=70 mm far from the quenching end, due to the long time in the

quenching sensitive range, the equilibrium phase precipitated in the crystal during the slow quenching process could be seen in Figure 8.5(b) and (c). The Fe-rich phase particles serve as the basis for inhomogeneous nucleation, which promotes the precipitation of the equilibrium phase Mg_2Si to a certain extent.

8.4.2 Effect of Quenching Cooling Rate on Mechanical Properties andMicrostructure of Alloys

The precipitation order of Al-Mg-Si alloy is: supersaturated solid solution α→GP region→β"→β'→β[25]. After aging at 180 °C for 5 h, many fine and uniform acicular dispersed phases β" were precipitated in the crystal as shown in Figure 8.6(a). Because the needle-like β" phase has a complete coherent relationship with the matrix, and basically has no mismatch with the matrix, β" is a monoclinic structure, and its lattice constants are: a=1.516 nm, b=0.405 nm, c= 0.674 nm (β=105.3°), the β" phase is the main precipitation strengthening phase in the Al-Mg-Si alloy, which has a good strengthening effect. The strength and hardness of the alloy largely depend on the aging precipitation phase β" size and volume fraction [26]. During the low-rate quenching process, the number of supersaturated solid solution and solute atoms in the alloy decreases, so that the strengthening precipitation phase β" decreases during the aging process. This is the main reason why the hardness of the aged state declines with the increase of the distance D from the quenching end [18]. Since the formation and continued growth of the coarse equilibrium phase during the quenching process consumes a large number of solute atoms in the matrix, the alloy has no aging precipitate in the area near the quenching precipitate during the subsequent aging process, but generates a certain width of PFZ, such as As shown in Fig. 8.8(d), this provides the quench sensitivity of the alloy. Compared to the matrix, the PFZ regions are much softer, so deformation preferentially occurs in these regions. This leads to dislocation cumulation and stress concentration, which degrades the mechanical properties of the alloy. The relationship between the Brinell hardness of 6082 aluminum alloy and the quenching cooling rate is revealed in Figure 9. It could be seen that when the quenching cooling rate of the alloy is lower than 5 °C/s, the aging Brinell hardness of the alloy decreases rapidly. (Reduced from 88 HB to 74 HB).

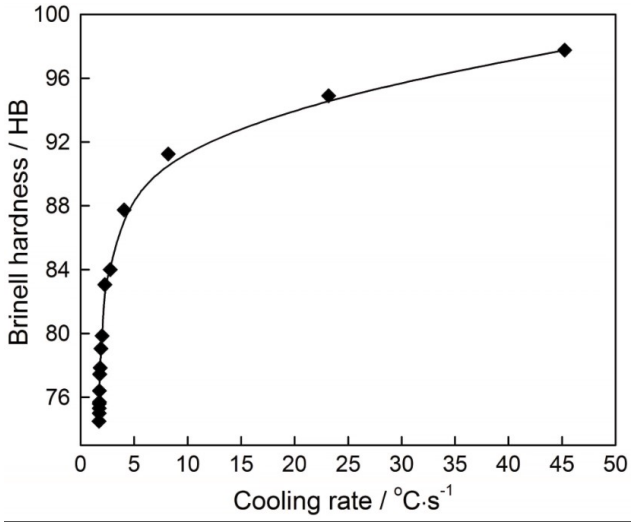

Fig.9 Brinell hardness of alloys determined by aging state and quenching cooling rate during quenching and aging process

In the defect structure of the alloy matrix, the interface has the highest energy, followed by other defects such as dislocations and vacancies, which are the specific nucleation sites of solid-state phase transformation. The β-equilibrium phase nucleates preferentially on grain boundaries and α-(AlMnFeSi) dispersions. In the subsequent aging process, the coarse β phase on the grain boundary consumes the solute atoms such as Mg and Si in the matrix, so that the equilibrium phase on the grain boundary becomes coarser and the quenching sensitivity of the alloy is improved. The width of the PFZ depends on the vacancy concentration, and the lower the vacancy concentration near the grain boundary, the wider the PFZ formed during the aging process. During the low-rate quenching process, more vacancies diffuse to the grain boundaries, forming a wider PFZ region, as shown in Fig.8. 7(c). In comparison with the matrix, the strength of PFZ at the grain boundary is lower, and it is easy to create uneven deformation during the stretching process. Therefore, dislocations tend to accumulate on PFZ, leading to stress concentration and crack initiation, reducing the hardness and strength of the alloy.

9. Conclusion

From the explanations in the previous eight chapters, it can be concluded:

1. The chemical composition affects the mechanical properties and temperature of heat treatment as well as the metallographic structure.
2. The temperature of heat treatment affects mechanical properties and metallographic structure.
3. The metallographic structure can reflect the mechanical properties, temperature and chemical composition.
4. The quenching sensitive temperature range of 6082 alloy is 220~425°C, and the critical quenching cooling rate must be higher than 6°C/s in the quenching sensitive range. The quenching depth of end-quenched 6082 aluminum alloy is 23 mm, and the quenching cooling rate at this time is 6.07°C/s, which is consistent with the results obtained by JMatpro7.0 simulation.

5. With the increase of the terminal quenching distance D, the reasons for the decline in the mechanical properties of the aging state are: 1) During the low-speed quenching process, the flaky β phase precipitates on the inhomogeneous dispersoid α-(AlMnFeSi) phase, and the β phase precipitates in the subsequent aging process. It grows up and absorbs the surrounding solute atoms, so that the degree of supersaturated solid solution of the alloy decreases and the strengthening phase β" of the intragranular precipitation decreases. 2) During the low-speed quenching process, the concentration of vacancies near the grain boundary declines, and the precipitation-free zone (PFZ) at the grain boundary expands.

10. References

1. Li Niankui, Nie Bo, Liu Jingan, Aluminum alloy materials and their heat treatment technology [M]. Beijing: Metallurgical Industry Press 2012: 200-234.
2. Wang Zhutang Heat Treatment Process of Deformed Aluminum Alloy[M]. Changsha City: Central South University Press 2011: 140-150114-134
3. Li Xuechao Microstructure and Metallographic Spectra of Aluminum Alloy Materials [M]. Beijing: Metallurgical Industry Press 2010: 46-62294-314.
4. Li Jionghui Metallographic Spectrum of Metal Materials [M]. Beijing: Machinery Industry Press 2006: 438-446.
5. Hu Yixiang, Metallographic Inspection Technology [M]. Beijing: Machinery Industry Press 2012: 113-123.
6. Wang Hongliang, Zeng Xianghao, Zhang Xinmeng, etc.Microstructure and properties of dissimilar friction stir welded joints of 5083 and 6061 aluminum alloys[J]. Journal of Materials Research, 2018, 32(6)
7. Ding Xiangqun, He Guoqiu, Chen Chengshu, etc.Research and application progress of 6000 series automotive aluminum alloys[J]. Chinese Journal of Materials Science and Engineering, 2005, 23(2): 302)
8. Antipov V.V., Klochkova Yu.Yu., Romanenko V.A. Modern aluminum and aluminum-silicon alloys. Aviation materials and technologies. 2017. No. S. p. 195-211.
9. Wen Liu, Wang Mengjun, Gao Meng, etc.Study on Quenching Sensitivity of 6061 Aluminum Alloy [J]. Journal of Materials Heat Treatment, 2014, 35(01): 94)
10. Filatov Yu.A. Works of VILSA on wrought aluminum alloys of the Al-Mg-Sc system. History of creation, structure, properties, application experience, problems and prospects. Light alloy technology. 2017. No. 3. p. 7-24.
11. Ber L.B. Patterns of structure formation in deformed semi-finished products from aluminum alloys / Technology of light alloys. 2014.No. 1. p. 5-31.
12. Rusakov G.M., Illarionov A.G., Loginov Yu.N., Lobanov M.L., Redikultsev A.A. Relationship between crystallographic grain orientations during hot deformation and recrystallization in aluminum alloy AMg6. Metal science and heat treatment of metals. 2014. No. 12 (714). p. 15-21.
13. Milevskaya T.V., Ruschits S.V., Tkachenko E.A., Antonov S.M. Deformation behavior of high-strength aluminum alloys under hot deformation conditions. Aviation materials and technologies. 2015. No. 2 (35). pp. 3-9.
14. Churyumov A.Yu., Bazlov A.I., Tsarkov A.A., Mikhailovskaya A.V. Study of the structure and properties of a wrought aluminum alloy of the Al-Mg-Mn system using the GLEEBLE 3800 complex for physical modeling of thermomechanical processes. Metallurgist. 2012. No. 8. p. 76-80.
15. Pesin A.M., Pustovoitov D.O., Vafin R.K. Modeling of temperature fields in the deformation zone during asymmetric rolling of aluminum alloys. Bulletin of the Magnitogorsk State Technical University. G.I. Nosov. 2015. No. 4 (52). pp. 75-81.
16. Golovnin M.A. Separation of the dynamic and static components of the load during sheet rolling of aluminum alloys. In the collection: Ural School of Young Metallurgists. Collection of materials and reports. 2017.
17. Golovnin M.A., Chernoskutova I.V. Deciphering the readings of the aluminum alloy hot rolling monitoring system. In the collection: Ural School of Young Metallurgists. Collection of materials and reports. 2015. p. 50-53
18. Loginov Yu.N., Seredkina M.Yu. Investigation of the high-speed rolling of an aluminum alloy slab using the FEM. lung technology alloys. 2015. No. 3. P. 121-126.
19. Loginov Yu.N., Golovnin M.A. Influence of the aluminum alloy hot slab rolling rate on the drive load. Rental production. 2016. No. 10. pp. 8-11.
20. Shang Baochuan, Yin Zhimin, Zhou Xiang, etc.Effects of solution-aging on the microstructure and properties of 6082 alloy extruded bars[J]. Journal of Materials Heat Treatment, 2011, 32(1): 77
21. Zhang Xinming, Ke Bin, Tang Jianguo, etc.Effect of Mn Content on Microstructure and Mechanical Properties of 6061 Aluminum Alloy[J]. Journal of Materials Research, 2013, (4): 337
22. Loginov Yu.N., Lobanov M.L., Golovnin M.A. A model for describing the deformation of aluminum alloys during their hot rolling, taking into account recrystallization processes. Blanking production in mechanical engineering. 2016. No. 9. pp. 32-36.
23. Churyumov A. Yu., Bazlov A. I., Tsarkov A. A., Mikhailovskaya A. V.Study of the structure and properties of a wrought aluminum alloy of the Al-Mg-Mn system using the GLEEBLE 3800 complex for physical modeling of thermomechanical processes. Metallurgist. 2012. No. 8. p. 76-80.
24. Loginov Yu.N., Golovnin M.A. A method for studying the rate hardening of an aluminum alloy during hot rolling. Metals. 2017. No. 2. pp. 33-38.
25. Loginov Yu.N., Golovnin M.A., Lobanov M.L., Doroshenko N.M. Investigation of the influence of technology for the production of flat products from an alloy of the Al-Si-Mg system on the anisotropy of properties. Light alloy technology. 2016. №3. pp. 69-74.
26. Danilov S.V., Reznik P.L., Lobanov M.L., Golovnin M.A., Loginov Yu.N. Influence of hot rolling on the anisotropy of the mechanical properties of aluminum alloy 6082. Bulletin of the South Ural State University. 2017. V. 17. No. 1. p. 73-80.
27. Gao Morita, Aluminum Alloy Technology [J]. Taipei: Gao Alumina Laser Technology Co., Ltd. 2014: 29-49.

****